

1 **Repurposing of drugs as novel influenza inhibitors from clinical gene** 2 **expression infection signatures**

3
4 **Authors:** Andrés Pizzorno^{1,2¶}, Olivier Terrier^{1¶*}, Claire Nicolas de Lamballerie^{1,3}, Thomas
5 Julien^{1,4}, Blandine Padey^{1,4}, Aurélien Traversier¹, Magali Roche³, Marie-Eve Hamelin², Chantal
6 Rhéaume², Séverine Croze⁵, Vanessa Escuret^{1,6}, Julien Poissy⁷, Bruno Lina^{1,6}, Catherine Legras-
7 Lachuer^{3,8}, Julien Textoris^{9,10}, Guy Boivin² and Manuel Rosa-Calatrava^{1,3*}.

8
9 ¹ Virologie et Pathologie Humaine - VirPath team, Centre International de Recherche en
10 Infectiologie (CIRI), INSERM U1111, CNRS UMR5308, ENS Lyon, Université Claude Bernard
11 Lyon 1, Université de Lyon, Lyon 69008, France.

12 ² Research Center in Infectious Diseases of the CHU de Quebec and Laval University, Quebec
13 City, QC G1V 4G2, Canada.

14 ³ Viroscan3D SAS, Lyon 69008, France.

15 ⁴ VirNext, Faculté de Médecine RTH Laennec, Université Claude Bernard Lyon 1, Université de
16 Lyon, Lyon 69008, France.

17 ⁵ ProfileXpert, SFR-Est, CNRS UMR-S3453, INSERM US7, Université Claude Bernard Lyon 1,
18 Université de Lyon, Lyon 69008, France.

19 ⁶ Laboratoire de Virologie, Centre National de Référence des virus Influenza Sud, Institut des
20 Agents Infectieux, Groupement Hospitalier Nord, Hospices Civils de Lyon, Lyon F-69317,
21 France.

22 ⁷ Pôle de Réanimation, Hôpital Roger Salengro, Centre Hospitalier Régional et Universitaire de
23 Lille, Université de Lille 2, Lille 59000, France.

24 ⁸ Ecologie Microbienne, UMR CNRS 5557, USC INRA 1364, Université Claude Bernard Lyon
25 1, Université de Lyon, Villeurbanne 69100, France.

26 ⁹ Service d'Anesthésie et de Réanimation, Hôpital Edouard Herriot, Hospices Civils de Lyon,
27 Lyon 69003, France.

28 ¹⁰ Pathophysiology of Injury-Induced Immunosuppression (PI3), EA 7426 Hospices Civils de
29 Lyon, bioMérieux, Université Claude Bernard Lyon 1, Hôpital Edouard Herriot, Lyon 69003,
30 France.

31

32 * Corresponding authors:

33 olivier.terrier@univ-lyon1.fr (OT), manuel.rosa-calatrava@univ-lyon1.fr (MRC)

34 ¶ These authors contributed equally to this work.

35

36 Text count: 6365 words

37 Inserts: 6 figures, 1 table, supplementary material

38

39 Keywords: Influenza viruses; antivirals; inhibitors of viral infection; transcriptome; host
40 targeting, drug repurposing

41

42 **Abstract**

43 **Background:** Influenza virus infections remain a major and recurrent public health burden. The
44 intrinsic ever-evolving nature of this virus, the suboptimal efficacy of current influenza
45 inactivated vaccines, as well as the emergence of resistance against a limited antiviral arsenal,
46 highlight the critical need for novel therapeutic approaches. In this context, the aim of this study
47 was to develop and validate an innovative strategy for drug repurposing as host-targeted
48 inhibitors of influenza viruses and the rapid evaluation of the most promising candidates in Phase
49 II clinical trials.

50 **Methods:** We exploited *in vivo* global transcriptomic signatures of infection directly obtained
51 from a patient cohort to determine a shortlist of already marketed drugs with newly identified,
52 host-targeted inhibitory properties against influenza virus. The antiviral potential of selected
53 repurposing candidates was further evaluated *in vitro*, *in vivo* and *ex vivo*.

54 **Results:** Our strategy allowed the selection of a shortlist of 35 high potential candidates out of a
55 rationalized computational screening of 1,309 FDA-approved bioactive molecules, 31 of which
56 were validated for their significant *in vitro* antiviral activity. Our *in vivo* and *ex vivo* results
57 highlight diltiazem, a calcium channel blocker currently used in the treatment of hypertension, as
58 a promising option for the treatment of influenza infections. Additionally, transcriptomic
59 signature analysis further revealed the so far undescribed capacity of diltiazem to modulate the
60 expression of specific genes related to the host antiviral response and cholesterol metabolism.
61 Finally, combination treatment with diltiazem and virus-targeted oseltamivir neuraminidase
62 inhibitor further increased antiviral efficacy, prompting rapid authorization for the initiation of a
63 Phase II clinical trial.

64 **Conclusions:** This original, host-targeted, drug repurposing strategy constitutes an effective and
65 highly reactive process for the rapid identification of novel anti-infectious drugs, with potential
66 major implications for the management of antimicrobial resistance and the rapid response to
67 future epidemic or pandemic (re)emerging diseases for which we are still disarmed.

68

69 **Background**

70 Besides their well-known pandemic potential, annual outbreaks caused by influenza viruses
71 account for several million respiratory infections and 250,000 to 500,000 deaths worldwide [1].
72 This global high morbidity and mortality of influenza infections represents a major and recurrent
73 public health threat with high economic burden. In this context, the suboptimal vaccine coverage
74 and efficacy, coupled with recurrent events of viral resistance against a very limited antiviral
75 portfolio, emphasize an urgent need for innovative treatment strategies presenting fewer
76 obstacles for their clinical use [2].

77 For decades, the strategy for antiviral development was mostly based on serial screenings of
78 hundreds of thousands of molecules to identify “hits” and ‘leads” that target specific viral
79 determinants, a quite costly and time-consuming process. However, the dramatic reduction in
80 successful candidate identification over time [3], along with a concomitant increase of regulatory
81 complexity to implement clinical trials, have fostered rising interest in novel strategies. Indeed,
82 new approaches, focused on targeting the host instead of the virus, as well as on marketed drug
83 repurposing for new antiviral indications [3–5] have been recently proposed in the context of
84 global health emergencies posed by Ebola [6] and Zika [7] viruses. Such innovative strategies
85 are strongly supported by a shift of paradigms in drug discovery, from “one-drug-one-target” to
86 “one-drug-multiple-targets” [8]. In that sense, different *in silico* approaches based on structural
87 bioinformatic studies [9, 10], systems biology approaches [11] and host gene expression analyses
88 [12] have been applied to decipher multi-purpose effects of many US Food and Drug
89 Administration (FDA)-approved drugs. Additionally, as successfully demonstrated in
90 antiretroviral therapy [13], targeting host instead of viral determinants may confer a broad-
91 spectrum antiviral efficacy, and also reduce the risk of emergence of drug resistance against

92 influenza viruses [14]. As a result, the last decade has witnessed several host-directed
93 experimental approaches against influenza infections, notably nitazoxanide, DAS181 or
94 acetylsalicylic acid [15–17].

95 In line with this emerging trend, we previously postulated that host global gene expression
96 profiling can be considered as a “fingerprint” or signature of any specific cell state, including
97 during infection or drug treatment, and hypothesized that the screening of databases for
98 compounds that counteract virogenomic signatures could enable rapid identification of effective
99 antivirals [18]. Based on this previous proof-of-concept obtained from *in vitro* gene expression
100 profiles, we further improved our strategy by analyzing paired upper respiratory tract clinical
101 samples collected during the acute infection and after recovery from a cohort of influenza
102 A(H1N1)pdm09-infected patients and determined their respective transcriptomic signatures. We
103 then performed an *in silico* drug screening using Connectivity Map (CMAP), the Broad
104 Institute’s publicly available database of more than 7,000 drug-associated gene expression
105 profiles [19, 20], and identified a list of candidate bioactive molecules with signatures anti-
106 correlated with those of the patient’s acute infection state (**Figure 1A**). The potential antiviral
107 properties of selected FDA-approved molecules were firstly validated *in vitro*, and the most
108 effective compounds were further compared to oseltamivir for the treatment of influenza
109 A(H1N1)pdm09 virus infections in both C57BL/6 mice and 3D reconstituted human airway
110 epithelia. Altogether, our results highlight diltiazem, a calcium channel blocker with so far
111 undescribed capacity to stimulate the epithelial antiviral defense, as a promising repurposed host-
112 targeted inhibitor of influenza infection. Moreover, our results plead in favor of the combination
113 of diltiazem with the virus-targeted antiviral oseltamivir for the improvement of current anti-
114 influenza therapy, and possibly decreasing the risk of antiviral resistance. This study confirms

115 the feasibility and interest of integrating clinical virogenomic and chemogenomic inputs as part
116 of a drug repurposing strategy to accelerate bedside-to-bench and bench-to-bedside drug
117 development.

118

119 **Methods**

120 **Clinical samples**

121 A previously published randomized clinical trial (ClinicalTrials.gov identifier NCT00830323)
122 was conducted in Lyon and Paris (France) during the peak circulation of the influenza
123 A(H1N1)pdm09 virus, with the aim to assess the efficacy of oseltamivir-zanamivir combination
124 therapy compared with oseltamivir monotherapy [21]. Briefly, patients tested positive for
125 influenza A infection by the QuickVue rapid antigen kit (Quidel) were randomized in one of the
126 two treatment groups and nasal wash specimens were collected within two hours of the first visit
127 and every 24 h until 96 h after treatment initiation. Nasal swabs were also performed on days 5
128 and 7. In voluntary patients, an optional supplementary nasal wash was performed at least three
129 months after influenza infection (recovery phase). H1N1 subtype was further confirmed by PCR.
130 For nine of these patients, transcriptomic data were obtained from paired samples collected
131 during influenza infection without treatment and in the recovery phase.

132

133 **Sample processing, RNA preparation and hybridization**

134 Nasal wash samples were collected in RNAlater® Stabilization Solution (Thermo Fisher
135 Scientific). Total RNA was extracted using RNeasy Micro kit (Qiagen) following the
136 manufacturer's instructions. RNA quality was assessed using a Bioanalyzer2100 (Agilent
137 technologies, Inc, Palo Alto, CA, USA). To account for samples having low amount and/or
138 partially degraded RNA (RNA Integrity Numbers between 1 and 8), we applied two types of
139 corrections: i) cRNA labelling was performed after a linear amplification protocol, as previously
140 described [22] and ii) raw signals obtained after hybridization of labelled cRNA on microarray

141 and data acquisition were processed using the MAXRS algorithm [23]. Labeled cRNA were
142 hybridized on Affymetrix HG-U133plus2 microarrays according to manufacturer's instructions
143 in a GeneChip® Hybridization Oven 640 (Affymetrix) and microarrays were subsequently
144 scanned in an Affymetrix 3000 7G scanner.

145

146 **Data normalization & MAXRS computational analysis**

147 The MAXRS algorithm [23] is particularly suited to gene expression analysis under low
148 hybridization conditions. Briefly, this method takes advantage of the specific design of
149 Affymetrix probe sets, which are composed of an average of 11 different probes that target the
150 same locus, and is based on the observation that for most of the probe sets the same probe shows
151 the highest fluorescence intensity in almost all arrays. For each microarray ($m = 1..M$) and for
152 each probeset ($t = 1..T$), fluorescence intensity values on microarray m of all probes ($p = 1..P_t$)
153 belonging to the probeset t are sorted in increasing order. These ranks are denoted as r_{mtp} . Then,
154 we calculated across all microarrays the rank sum (RS_{tp}) for each probeset t for each probe p
155 belonging to the probeset t . Finally, for each probeset t , we kept the three probes p with the
156 highest RS_{tp} . The mean intensity of these three probes is attributed to the probeset t . As it is
157 common practice with many modern pre-processing algorithms, and because of the low global
158 fluorescence signal intensity, mismatched probes were excluded from MAXRS analysis.

159 After pre-processing the raw dataset with the MAXRS algorithm, a normalization step was
160 performed using Tukey median-polish algorithm [24]. Differential expression was assessed by
161 applying a Student t-test for each probeset, and multiple testing was corrected using the
162 Benjamini-Hochberg algorithm in the qvalue library [25]. For further downstream analysis,
163 genes were selected according to two criteria: i) absolute fold change >2 , and ii) corrected p-

164 value <0.05. Data were generated according to the Minimum Information About a Microarray
165 Experiment guidelines and deposited in the National Center for Biotechnology Information's
166 Gene Expression Omnibus [26] under accession number GSE93731.

167

168 **Functional analysis**

169 Functional enrichment analysis was performed on a selection of differentially-expressed genes
170 with DAVID tools [27], using the Gene Ontology (GO) [28]. To further select genes for the
171 CMAP query, we selected 6 Biological Process terms (GO_BP: GO:0009615-response to virus;
172 GO:0006955-immune response; GO:0042981-regulation of apoptosis; GO:0006952-defense
173 response; GO:0009611-response to wounding; GO:0042127-regulation of cell proliferation) that
174 shared > 90% of genes with all significantly enriched GO_BP terms, and 3 relevant Cellular
175 Component terms (GO_CC: GO:0031225-anchored to membrane; GO:0005829-cytosol;
176 GO:0005654-nucleoplasm). To visualize and compare the different lists of compounds, Venn
177 diagrams were obtained using the webtool developed by Dr. Van de Peer's Lab at Ghent
178 University (<http://bioinformatics.psb.ugent.be/webtools/Venn/>).

179

180 **Cells and viruses**

181 Human lung epithelial A549 cells (ATCC CCL-185) were maintained in Dulbecco's modified
182 Eagle's medium (DMEM) supplemented with 10 % foetal calf serum and supplemented with 2
183 mM L-glutamine (Sigma Aldrich), penicillin (100 U/mL) and streptomycin (100 µg/mL)
184 (Lonza), maintained at 37 °C and 5% CO₂.

185 Influenza viruses A/Lyon/969/09 and A/Quebec/144147/09 were produced in MDCK (ATCC
186 CCL-34) cells in EMEM supplemented with 2 mM L-glutamine (Sigma Aldrich), penicillin (100
187 U/mL), streptomycin (100 µg/mL) (Lonza) and 1 µg/mL trypsin. Viral titers in plaque forming
188 units (PFU/ml) and tissue culture infectious dose 50% (TCID50/mL) were determined in MDCK
189 cells as previously described [29, 30].

190

191 **Viral growth assays**

192 For viral growth assays in the presence of molecules, A549 cells were seeded 24 h in advance in
193 multi-well 6 plates at 1.8×10^5 cells/well. Three treatment protocols were evaluated. 1) In pre-
194 treatment protocol, cells were washed with DMEM and then incubated with different
195 concentrations of candidate molecules diluted in DMEM supplemented with 2 mM L-glutamine
196 (Sigma Aldrich), penicillin (100 U/mL), streptomycin (100 µg/mL) (Lonza) and 0.5 µg/mL
197 trypsin. Six hours after treatment, cells were washed and then infected with A/Lyon/969/09
198 (H1N1)pdm09 virus at a MOI of 0.1. 2) In pre-treatment plus post-treatment protocol, cells were
199 initially treated and infected in the same conditions as explained above. One hour after viral
200 infection, a second identical dose of candidate molecules in supplemented DMEM was added. 3)
201 In post-treatment protocol, cells without pre-treatment were infected in the conditions described
202 and treatments with candidate molecules at the indicated concentrations were initiated 24 h p.i.
203 In all cases, supernatants were collected at 48 h p.i. and stored at -80 °C for TCID50/ml viral
204 titration.

205 **Viability and cytotoxicity assays**

206 Cell viability was measured using the CellTiter 96® AQueous One Solution Cell Proliferation
207 Assay (MTS, Promega). A549 cells were seeded into 96-well plates and treated with different
208 concentrations of molecules or solvents. Cells were incubated at 37 °C and 5% CO₂ and then
209 harvested at different time-points, following the same scheme as in viral growth assays. Results
210 were presented as a ratio of control values obtained with solvents. Treatment-related toxicity in
211 human airway epithelia (HAE) was measured using the Cytotoxicity Detection Kit^{PLUS} (LDH,
212 Roche) according to the manufacturer's instructions. Briefly, duplicate 100 µL-aliquots of
213 basolateral medium from treated and control HAEs were incubated in the dark (room
214 temperature, 30 minutes) with 100 µL of lactate dehydrogenase (LDH) reagent in 96-well plates.
215 After incubation, "stop solution" was added and the absorbance was measured in a conventional
216 microplate ELISA reader. The photometer was set up for dual readings to determine non-specific
217 background at 750 nm, and absorbance was measured at 490 nm. Percent cytotoxicity was
218 calculated as indicated by the manufacturer, using mock-treated and 1% triton-treated epithelia
219 as "low" and "high" controls, respectively. Percent viability is presented as 100 – percent
220 cytotoxicity.

221

222 **Mouse model of viral infection**

223 All protocols were carried out in seven to nine-week old female C57BL/6N mice (Charles River,
224 QC, Canada). Animals were randomized in groups of 15 according to their weight to ensure
225 comparable median values on each group, and then housed in micro-isolator cages (5 animals per
226 cage) in a biosafety 2 controlled environment (22 °C, 40% humidity, 12:12 h photoperiods), with
227 *ad libitum* access to food and water.

228 On day 0, mice were lightly anesthetized with inhaled 3% isoflurane/oxygen, and then infected
229 by intranasal (i.n.) instillation of influenza A/Quebec/144147/09 (H1N1)pdm09 virus in 30 µl of
230 saline, as specified in each case. Control animals were mock-infected with 30 µl of saline.
231 Candidate molecules were evaluated in two different treatment protocols: i) treatments were
232 started on the same day of infection (day 0, 6 h prior to infection), or ii) treatments were started
233 24 h after infection (day 1). Regardless of treatment initiation time, all treatments were
234 performed *per os* (150-µl gavage) once daily for 5 consecutive days (5 drug administrations in
235 total). Mortality, body weight and clinical signs such as lethargy and ruffled fur were daily
236 monitored on 10 animals/group for a total of 14 days. Animals were euthanized if they reached
237 the humane endpoint of >20% weight loss. The remaining 5 animals/group were euthanized on
238 day 5 p.i. to measure LVTs.

239 Vehicle (saline) or oseltamivir were used as placebo and positive treatment control, respectively.
240 The oseltamivir dose (10 mg/kg/day) was adjusted to confer ~50% protection in the selected
241 experimental conditions and is considered a good correlate of half the normal dose of 150
242 mg/day given to humans [31]. The doses of repurposed candidate molecules were selected to be
243 in the non-toxic range for mouse studies, according to published preclinical data for their first
244 therapeutic indication. To validate this choice in our specific model, potential drug toxicity was
245 evaluated in mock-infected animals treated with the same regimens as virus-infected mice.

246

247 **Pulmonary viral titers**

248 In order to evaluate the effect of different treatments on viral replication, 5 animals per group
249 were euthanized on day 5 p.i. and lungs were removed aseptically. Mice were randomly selected
250 from the 3 cages of each group to minimize cage-related bias. Lungs were homogenized in 1 ml

251 of PBS using a bead mill homogenizer (Tissue Lyser, Qiagen) and debris was pelleted by
252 centrifugation (2,000 g, 5 min). Triplicate 10-fold serial dilutions of each supernatant were plated
253 on ST6GalIMDCK cells (kindly provided by Dr. Y. Kawaoka, University of Wisconsin,
254 Madison, WI) and titrated by plaque assays [29]. The investigator was blinded to group
255 allocation.

256

257 **Viral infection in reconstituted human airway epithelium (HAE)**

258 MucilAir® HAE were obtained from Epithelix SARL (Geneva, Switzerland) and maintained in
259 air-liquid interphase with specific culture medium in Costar Transwell inserts (Corning, NY,
260 USA) according to manufacturer's instructions. For infection experiments, apical poles were
261 gently washed with warm PBS and then infected with a 100- μ L dilution of influenza
262 A/Lyon/969/09 (H1N1)pdm09 virus in OptiMEM medium (Gibco, ThermoFisher Scientific) at a
263 MOI of 0.1. Basolateral pole sampling as well as 150- μ L OptiMEM apical washes were
264 performed at the indicated time points, and then stored at -80 °C for PFU/mL and TCID₅₀/mL
265 viral titration. Treatments with specific dilutions of candidate molecules alone or combined with
266 oseltamivir in MucilAir® culture medium were applied through basolateral poles. All treatments
267 were initiated on day 0 (5 h after viral infection) and continued once daily for 5 consecutive days
268 (5 drug administrations in total). Variations in transepithelial electrical resistance (Δ TEER) were
269 measured using a dedicated volt-ohm meter (EVOM2, Epithelial Volt/Ohm Meter for TEER)
270 and expressed as Ohm/cm².

271

272 **High throughput sequencing and bioinformatics analysis**

273 cDNA libraries were prepared from 200 ng of total RNA using the Scriptseq™ complete Gold
274 kit-Low Input (SCL6EP, Epicentre), according to manufacturer's instructions. Each cDNA
275 library was amplified and indexed with primers provided in the ScriptSeq™ Index PCR Primers
276 kit (RSBC10948, Epicentre) and then sequenced as 100 bp paired-end reads. Prior to sequencing,
277 libraries were quantified with QuBit and Bioanalyzer2100, and indexed libraries were pooled in
278 equimolar concentrations. Sequencing was performed on an Illumina HiSeq 2500 system
279 (Illumina, Carlsbad, CA), with a required minimum of 40 million reads sequenced per sample.
280 Conversion and demultiplexing of reads was performed using bcl2fastq 1.8.4 (Illumina). The
281 FastQC software (<http://www.bioinformatics.babraham.ac.uk/projects/fastqc>) was used for
282 quality controls of the raw data. Reads were trimmed using the Trimmomatic [32] software, with
283 a minimum quality threshold of Q30. Trimmed reads were pseudo-aligned to the *Homo sapiens*
284 genome (GRCh38.p11) using the Kallisto software [33]. Statistical analysis was performed in
285 R3.3.1 with the package EdgeR 3.14.0 [34]. Differential expression was calculated by comparing
286 each condition to the mock using a linear model. The Benjamini-Hochberg procedure was used
287 to control the false discovery rate (FDR). Transcripts with an absolute fold change >2 and a
288 corrected p-value <0.05 were considered to be differentially expressed. Enriched pathways and
289 GO terms were assessed with DAVID 6.8 [27]. For visualization purposes, a heatmap and
290 stacked barplots were constructed in R3.3.1 on mean-weighted fold changes and association
291 between conditions were assessed by Spearman correlation analysis.

292

293 **Statistical analysis**

294 All experimental assays were performed in duplicate at a minimum, and representative results
295 are shown unless indicated otherwise. No statistical methods were used to predetermine sample

296 size in animal studies, which were estimated according to previous studies and the known
297 variability of the assays. No mice were excluded from post-protocol analyses, the experimental
298 unit was an individual animal and equal variance was assumed. Kaplan-Meier survival plots
299 were compared by Log-Rank (Mantel-Cox) test and hazard ratios (HR) were computed by the
300 Mantel-Haenszel method. Weight loss and viral titers of all groups were compared by one-way
301 analysis of variance (ANOVA) with Tukey's multiple comparison post-test. The testing level (α)
302 was 0.05. Statistical analyses were performed on all available data, using GraphPad, Prism 7.

303

304

305 **Results**

306 **Generation of clinical virogenomic profiles.** We determined *in vivo* transcriptional signatures
307 of infection from paired nasal wash samples of nine untreated patients, collected during acute
308 A(H1N1)pdm09 pandemic influenza infection (“infected”) and at least three months later to
309 ensure a recovery non-infected state (“cured”) [21]. The nine patients from whom transcriptomic
310 data could be obtained constitute a representative sample of the whole studied cohort, except for
311 the male sex ratio (**Table S1**). We combined two strategies to tackle the characteristic low RNA
312 amount/quality of this type of clinical samples. Firstly, cRNA labelling was performed after a
313 linear amplification of initial RNA, as previously described [35]. Secondly, raw signals obtained
314 after hybridization of labelled cRNA on microarray and data acquisition were processed using
315 the MAXRS algorithm [23] to overcome low hybridization conditions. This approach, initially
316 developed for the analysis of heterologous hybridizations, takes advantage of the specific design
317 of the Affymetrix® microarray used in our study, with several probes targeting the same locus
318 [23].

319 After normalization, differentially expressed genes were selected based on two criteria: i) an
320 absolute fold change >2 , and ii) a Benjamini-Hochberg corrected p-value <0.05 . We therefore
321 identified a total of 1,117 commonly deregulated probes, with almost equal proportion of up-
322 regulated (48.4%; n=541) and down-regulated probes (51.7%; n=576). Remarkably, despite
323 considerable inter-patient variability among recovery state samples, a substantial homogenization
324 of transcriptional profiles was observed in the context of infection, as shown in the heatmap
325 presented in **Figure 1B** and by the median Spearman’s ρ correlation values for both groups (0.60
326 “cured” vs. 0.90 “infected”). These virogenomic signatures of infection constituted the input for
327 the subsequent *in silico* query for the identification of candidate compounds.

328

329 ***In silico* cross-analysis of chemogenomic versus virogenomic clinical profiles.** We then
330 performed an *in-silico* search for molecules that reverse the virogenomic signature of infection,
331 using the CMAP database (Build 02) as previously described [18]. CMAP is a collection of
332 genome-wide transcriptional expression data from cultured human cells treated with bioactive
333 small molecules. HG-U133plus2 probesets were mapped to the U133A probesets using the
334 Ensembl BioMarts online tool [36, 37], and connectivity scores and p-values were obtained
335 using the CMAP algorithm [19, 20]. With the global set of 1,000 most differentially expressed
336 genes as input (**Figure 1C**, Main List), we obtained a preliminary list of 60 candidate
337 compounds. In parallel, we used two other subsets of genes belonging to significantly enriched
338 Gene Ontology (GO) terms obtained from microarray analyses to introduce functional bias and
339 add more biological significance to our first screening. Hence, by using 6 Biological Process
340 terms (GO_BP) that shared more than 90% of genes (**Figure 1C**, Functional cross-analysis #1), a
341 second list of 109 compound candidates was obtained. A third list of 19 compounds was
342 obtained using 3 relevant Cellular Component terms (GO_CC) (**Figure 1C**, Functional cross-
343 analysis #2). The comparison of the 160 compounds from the three distinct lists (12.2% of
344 compounds of CMAP, **Table S2**) highlighted monensin as the only common compound (**Figure**
345 **1D**).

346 To rationally reduce the number of drug candidates, bioactive drugs were excluded if not
347 compatible with a final use as antiviral, mostly for safety (e.g. teratogens, intercalating agents)
348 and/or pharmacological (e.g. documented low bioavailability) reasons, based on clinical data and
349 the PubMed/PubChem databases. Thus, the number of candidates was initially decreased to 139
350 and then to 110 (**Figure S1**). We subsequently determined a shortlist of 35 bioactive molecules

351 (<3% of CMAP, **Table 1**) for *in vitro* screening, based on two main criteria: i) molecules
352 representative of the different pharmacological classes identified, and ii) molecules evenly
353 distributed in the three lists obtained after *in silico* screening (Main List, List #1 and List #2,
354 **Figure 1D**), which comprise a panoply of documented pharmacological classes, including anti-
355 fungal agents (e.g. monensin, flucytosine), anti-inflammatory agents (e.g. felbinac, apigenin,
356 prednisone) and adrenergic agonists/antagonists (timolol, methoxamine, tolazoline), as
357 represented in the Venn diagram (**Figure 1D, Table 1**). Interestingly, at least 14 (40%)
358 molecules from our short-list belong to a pharmacological class related with anti-microbial or
359 anti-inflammatory activities (**Table 1, #**), and 11 (31.4%) have already been reported in the
360 literature for their antiviral properties against influenza or other viruses (**Table 1, ***), notably the
361 nucleoside inhibitor ribavirin [38, 39] and the ionophore monensin [40].

362

363 **Inhibitory effect of the selected molecules on A(H1N1)pdm09 viral growth *in vitro*.** *In vitro*
364 screening of the antiviral potency of the 35 selected molecules was performed in A549 human
365 lung epithelial cells seeded in 6-well plates. Firstly, we evaluated the impact of 6 h pre-treatment
366 with a 10-fold drug concentration range, using the original CMAP concentration as reference.
367 Six hours after treatment, cells were washed and infected with influenza A(H1N1)pdm09 virus at
368 a multiplicity of infection (MOI) of 0.1. Viral titers in supernatants collected from treated
369 samples at 48 h post infection (p.i.) were normalized with those measured in mock-treated
370 controls ($>10^5$ TCID₅₀/mL). Potential treatment-induced cell toxicity was evaluated in the same
371 experimental conditions using the MTS assay and expressed also as the percentage of cell
372 viability compared to non-infected controls (**Figure 2**). Based on antiviral activity and cell
373 viability profiles obtained (**Figure 2A**, blue triangles), we defined as “inhibitors” compounds

374 that fulfilled the following two criteria: i) induce >75% reduction on viral production, and ii)
375 have minor impact on cell viability, with relative values in the 90%-110% range (**Figure 2A**,
376 squares in **left panels** and zooms in **right panels**). A total of 10 compounds (28.6%) matched
377 both criteria, mainly when used at a 10-fold CMAP concentration (**Figure 2B**), yet only a limited
378 number of them exhibited classic dose-dependent inhibition. Whenever possible, as in the case of
379 monensin or ranitidine for example, EC50 values were calculated, which were mostly in the
380 micromolar range (**Figure 2B**).

381 In a second round of screening, we tested the same 6 h pre-treatment but with serial 10-fold
382 dilutions from the initial CMAP concentration to CMAP/10,000, followed by one additional
383 treatment immediately after infection (**Figure 2A**, green circles in **left and right panels**). In
384 these conditions, 30 compounds (85.7%) met our criteria to be considered as inhibitors of viral
385 production (**Figure 2C**), with half of them showing a classic dose-dependent inhibition effect.
386 Calculated EC50 values were in the nanomolar range and hence significantly lower than those
387 calculated in the context of pre-treatment only. Dose response curves and calculated EC50 for all
388 the 35 compounds are presented in **Figure S2** and **Table S3**, respectively.

389

390 **Efficacy of selected molecules for the treatment of influenza A(H1N1)pdm09 virus infection**
391 **in mice.** Based on EC50 and cytotoxicity data from the *in vitro* screening, we selected 8 molecules
392 to investigate their potential as inhibitors of influenza A(H1N1)pdm09 in C57BL/6 mice.
393 Oseltamivir, the standard antiviral for the treatment of influenza infections was used as control.
394 All treatments were performed *per os*, starting 6 h before infection and being continued once
395 daily for 5 consecutive days (5 drug administrations in total) (**Figure 3**). While animals treated
396 with oseltamivir or monensin showed clinical improvement compared to the saline (placebo)

397 group in terms of survival and weight loss (oseltamivir only), treatment with Lanatoside C,
398 prednisolone, flucytosine, felbinac and timolol showed no clinical benefit at the selected
399 concentrations (**Figure S5A**). In contrast, diltiazem and etilefrine not only significantly
400 improved survival and maximum mean weight losses (**Figure 3A-B**), but also showed at least 1-
401 log reductions in lung viral titers (LVTs) on day 5 p.i. (**Figure 3C**). Importantly, no signs of
402 toxicity were observed for any of the drugs at the regimens tested (**Figure S3B**).

403

404 **Diltiazem retains its *in vivo* efficacy when administered 24 h after viral infection.** To best
405 mimic the therapeutic setting, we next evaluated the efficacy of the same 5-day oral regimen
406 with diltiazem or etilefrine but when initiated 24 h after viral infection (**Figure 4**). As with
407 oseltamivir and monensin, diltiazem treatment completely prevented mortality and reduced
408 weight loss in influenza A(H1N1)pdm09 infected mice, which otherwise showed only 50%
409 (5/10) survival for the etilefrine and saline groups (**Figure 4A-B**). Interestingly, 1- to 1.5-log
410 reductions in LVTs compared to the saline group were observed at day 5 in groups of mice
411 treated with diltiazem or etilefrine (**Figure 4C**). We then used a more stringent approach by
412 increasing the viral inoculum to evaluate the same delayed (24 h post infection) 5-day diltiazem
413 regimen in the context of a 100% lethal A(H1N1)pdm09 infection (**Figure 4D-F**). Whereas
414 treatment with oseltamivir and diltiazem successfully rescued 40% (4/10) and 20% (2/10) of
415 mice, respectively, half-dose treatment with diltiazem (45 mg/kg) rescued 30% (3/10) of mice
416 from death, also showing significant improvement in mean weight loss (**Figure 4D-E**).
417 Calculated hazard ratios (HR) for the saline group compared to these three treatment groups were
418 8.41 (CI95: 1.65-43.02), 2.85 (0.56-14.47) and 7.62 (1.49-38.96), respectively. Noteworthy,
419 LVTs at day 5 p.i. were comparable among all treated and untreated groups (**Figure 4F**),

420 suggesting mainly a protective effect of diltiazem towards severe influenza infection rather than
421 a direct role in decreasing viral production.

422

423 **Diltiazem significantly reduces viral replication in infected reconstituted human airway**
424 **epithelia (HAE).** To further complement *in vivo* data, we characterized the inhibitory properties
425 of diltiazem using a biologically relevant reconstituted airway epithelium model, derived from
426 human primary bronchial cells (MucilAir®, Epithelix). HAE were infected with influenza
427 A(H1N1)pdm09 at a MOI of 0.1, and treatments on the basolateral medium were initiated 5 h p.i.
428 and continued once daily for 5 consecutive days. In the absence of treatment, viral replication at
429 the apical surface peaked at 48 h p.i. ($\sim 1 \times 10^8$ PFU/ml) and was detectable at important levels
430 for at least 7 days. As expected, trans-epithelial electrical resistance (TEER) values, measuring
431 tight junction and cell layer integrity, sharply decreased and bottomed out at 72 h p.i. in the
432 untreated control, correlating with the first virus detection on the basolateral medium (**Figure 5A**
433 **and Table S6**). A similar pattern was observed in infected HAE treated with oseltamivir 0.1 μ M
434 or diltiazem 9 μ M (CMAP), which conferred no significant advantage over the untreated control.
435 Conversely, oseltamivir 1 μ M and diltiazem 90 μ M treatments (10-fold CMAP) strongly
436 inhibited viral replication, delaying the peak of viral production by 24 h. Both treatments induced
437 >3-log reductions in apical viral titers at 48 h p.i. compared to the untreated control, and >2-log
438 reductions when comparing peak titers (48 h p.i. untreated vs. 72 h p.i. treated). Moreover,
439 whereas oseltamivir treatment stabilized TEER during the time-course of infection, diltiazem
440 treatment partially buffered the TEER decrease observed in the untreated control (**Figure 5A** and
441 **Table S6**). No virus was detected on the basolateral medium for these two treated groups, and
442 absence of treatment-induced toxicity was confirmed by measuring the release of intracellular

443 lactate dehydrogenase (LDH). Interestingly, we observed that inhibitory and protective
444 properties demonstrated by diltiazem were progressively reversible when basolateral medium
445 was replaced with fresh medium without drugs. Overall, these results are in accordance and
446 strongly support the inhibitory and protective effects of diltiazem observed *in vitro* and in mice,
447 respectively.

448

449 **Diltiazem-oseltamivir combination confers improved efficacy when compared to**
450 **monotherapy in infected HAE.** We anticipated that the combination of two antiviral
451 compounds that target different viral/cellular determinants could induce better virological and
452 physiological responses when compared to antiviral monotherapy. We therefore evaluated the
453 diltiazem-oseltamivir combination in the same conditions described above, notably a 5-day
454 treatment course with treatment initiation at 5 h p.i. The diltiazem 90 μM / oseltamivir 1 μM
455 combination conferred >3-log reduction in apical peak viral titers when compared to the
456 untreated control, even greater than that observed with same dose monotherapy. TEER values
457 remained stable during combined treatment, comparable to those observed with oseltamivir 1
458 μM monotherapy (**Figure 5B** and **Table S6**). Remarkably, although not effective as
459 monotherapy in the low concentrations tested above, the diltiazem 9 μM / oseltamivir 0.1 μM
460 combination contrariwise delayed the peak of viral production, significantly reduced apical viral
461 titers, and slightly buffered TEER values compared to the untreated control (**Figure 5B** and
462 **Table S6**). Once again, no treatment-related toxicity was observed for any of the combinations
463 tested. These results plead in favor of the potential of diltiazem for the improvement of current
464 anti-influenza therapy with neuraminidase inhibitors.

465

466 **Diltiazem treatment induces a significant reversion of the viral infection signature.** Since
467 the rationale behind our approach relies on attaining antiviral activity through a drug-induced
468 global and multi-level inversion of the infection signature, we advantageously used the
469 MucilAir® HAE model coupled with high-throughput sequencing in order to characterize and
470 compare the specific transcriptional signatures induced by infection and/or diltiazem treatment
471 (**Figures 6 and S4**). HAE were mock-infected or infected with influenza A(H1N1)pdm09 virus
472 and then mock-treated or treated in the same experimental conditions in which the antiviral effect
473 of diltiazem has been previously validated (MOI of 0.1, 90 μ M diltiazem). At 72 h p.i., cells
474 were lysed and total RNA was extracted. cDNA libraries were then produced, amplified, and
475 subjected to high-throughput sequencing. Taking the mock-infected / mock-treated (“mock”) as
476 baseline, we initially performed DAVID functional gene enrichment (absolute fold change >2,
477 Benjamini-Hochberg corrected p-value <0.05) on the specific transcriptional signature of
478 diltiazem with the objective of gaining insight on the putative host pathways involved in its
479 antiviral effect. The lists of up-regulated (n=194) and down-regulated (n=110) transcripts in the
480 mock-infected / diltiazem (“mock + diltiazem”) condition were analyzed using DAVID 6.8 to
481 highlight associations with specific GO terms. Although no enriched BP was identified among
482 down-regulated transcripts, the list of up-regulated transcripts associated with diltiazem
483 treatment highlighted 7 particularly enriched BP. While 4 of these BP (GO:0009615;
484 GO:0045071; GO:0051607; GO:0060337) are directly linked to antiviral response/cellular
485 response to virus, the remaining 3 (GO:0055114; GO:0008299; GO:0006695) are involved in
486 cholesterol biosynthesis/metabolism (**Figure 6A**). We then compared the common differentially
487 expressed transcript levels between the three infection/treatment conditions. These
488 transcriptional signatures revealed a marked anti-correlated profile between the “mock +

489 diltiazem” and the infected / mock-treated (“H1N1”) conditions (**Figure 6B**), supported by a
490 median Spearman’s ρ correlation value of -0.82 (**Figure 6C**). Most important, the infected /
491 diltiazem (“H1N1 + diltiazem”) condition yielded ρ correlation values of 0.40 and -0.72 when
492 compared to either “mock + diltiazem” or “H1N1”, respectively, therefore confirming a partial
493 reversion of the infection virogenomic signature during effective antiviral treatment with
494 diltiazem (**Figures 6D and S4**), as expected.

495

496

497 **Discussion**

498 The existing urge for alternative strategies to cope with the limited efficacy of currently
499 approved antivirals for the prevention and treatment of influenza infections [2, 41, 42], mostly in
500 the case of patients with severe influenza and acute respiratory distress syndrome (ARDS) [43,
501 44], represented the central driving force of this study. Here, we developed and validated for the
502 first time an innovative approach based on clinical genomic signatures of respiratory viral
503 infections for the rapid discovery, *in vitro*, *in vivo* and *ex-vivo* evaluation, as well as the
504 repurposing of FDA-approved drugs for their newly identified host-targeted inhibitory and
505 protective properties against influenza infections.

506 Targeting host components on which viral replication depends instead of viral determinants
507 represents a real change of paradigm in antiviral development, with pioneering results mainly
508 observed in the context of antiretroviral therapy [13, 45]. Nevertheless, and despite strong
509 putative advantages such as the achievement of broad-spectrum antiviral efficacy and the
510 minimization of viral drug resistance, this approach usually fails to overcome two major limiting
511 factors of classic compound screening. Firstly, it remains target-centered *per se*, therefore
512 leading to the identification of drugs with limited efficacy due to the complex network and high
513 redundancy of the host cellular pathways. Secondly, the need of high-throughput screenings
514 often entails the measurement of a very limited number of viral parameters, usually in non-
515 physiologically and hence poorly relevant conditions and/or cellular models.

516 Based on our initial proof-of-concept study on the *in silico* screening of the CMAP database [19,
517 20] with no initial *a priori* on specific host targets [18], we moved our approach up to the clinical
518 trial setting, by determining exploitable and more relevant virogenomic profiles directly from

519 standard clinical samples of influenza-infected patients. Since the low amount of often degraded
520 RNA obtained from these samples represented a major challenge, we implemented an original
521 combination of sample preparation techniques for low input but high quality samples with data
522 processing initially designed for expression analysis of non-model species [22, 23].

523 Another substantial development was the integration of several lists of candidate molecules
524 issued from different transcriptomic signatures with enriched relevant DAVID Gene Ontology
525 terms, and their final selection based on their pharmacological classes and potential compatibility
526 as antivirals. Our refined strategy allowed the selection of a shortlist of 35 high potential
527 candidates out of a rationalized computational screening of a total of 1,309 FDA-approved
528 bioactive molecules. This drastic positive selection step constituted a major advantage, since it
529 enabled the implementation of relevant and integrated *in vitro*, *in vivo* and *ex-vivo* evaluations in
530 a time- and cost-effective manner. Most important, the use of patient (*in vivo*) virogenomic
531 profiles led to the identification of molecules with highly improved *in vitro* activity and
532 significant *in vivo* antiviral efficacy as compared with compounds previously obtained from our
533 initial study based on cell culture (*in vitro*) virogenomic profiles [18]. These results truly
534 highlight the added value of using relevant clinical virogenomic signatures to optimize the
535 computational screening for active drugs.

536 Two of the molecules identified in this study with transcriptomic profiles that counteract clinical
537 virogenomic signatures (e.g. ribavirin and monensin) have already been validated for their anti-
538 influenza properties [38, 40], and then supported the relevance of our compound selection
539 strategy. Nevertheless, although different modes of action have been postulated for the anti-
540 influenza activity of the synthetic guanosine analog ribavirin [39], the exact mechanisms remain
541 uncharacterized so far. Similarly, it has been postulated that monensin, an antibiotic isolated

542 from *Streptomyces spp*, may have a role as a ionophore that interferes with intracellular transport
543 of several enveloped viruses, including influenza [40]. In that sense, even if we cannot rule out
544 that some of the molecules identified *in silico* exert a direct effect on a specific pathway or
545 cellular target, the fact that these molecules have been identified with a high anti-correlation rate
546 in CMAP strongly supports a potential multi-target inhibitory effect, probably resulting in deep
547 modifications of host gene expression. In fact, both monensin and ribavirin were previously
548 reported to modulate the host cellular gene expression profile, notably through the up-regulation
549 of the cholesterol and lipid biosynthesis genes [46] or the virus-induced ISRE signaling and
550 antiviral ISGs genes [47], respectively.

551 The two most promising molecules highlighted in this study are etilefrine, an alpha and beta-
552 adrenergic receptor agonist, currently indicated as a cardiogenic and anti-hypotensive agent [48]
553 and mainly diltiazem, a voltage-gated Ca²⁺ channel antagonist that is currently used to control
554 angina pectoris and cardiac arrhythmia [49]. In addition to their strong inhibitory effect on the
555 viral growth of circulating A(H1N1)pdm09 viruses, with *in vitro* EC50 values in the nanomolar
556 range (**Figure 2**), both molecules also demonstrated antiviral properties against oseltamivir-
557 resistant A(H1N1)pdm09 and prototype H3N2 and B influenza strains (**Table S4**). Our *in vivo*
558 results (**Figures 3-4**), obtained without previous treatment optimization in terms of dosage or
559 administration route, also suggest that these drugs harbor a protective role towards influenza
560 infection, particularly in the case of diltiazem, which conferred increased survival in mice even
561 in a model of severe influenza infection (**Figure 4D-F**). Moreover, the inhibitory and protective
562 properties of diltiazem were validated in the reconstituted human airway epithelium model, also
563 showing enhanced efficacy when combined with oseltamivir (**Figure 5**).

564 Finally, a very recent study by Fujioka and colleagues [50] confirmed the antiviral activity of
565 diltiazem anticipated by our approach. In that study, based on the role of Ca²⁺ channels on the
566 attachment of influenza viruses to the host cell, the authors discuss whether the diltiazem
567 induced modulation of Ca²⁺ channel activity might not fully explain such observed antiviral
568 activity, consistent with a multi-level (off-target) effect of diltiazem. In this context, in which not
569 all Ca²⁺ channel inhibitors confer significant antiviral activity, the newly described capacity of
570 diltiazem to partially reverse the global virogenomic signature of infection and modulate specific
571 genes related to the host antiviral response and cholesterol metabolism (**Figures 6 and S4**)
572 suggests a putative explanation for its inhibitory effect observed *in vitro*, *ex vivo* and in mice.
573 Nevertheless, further investigations are underscored to shed light on the specific mechanisms
574 underlying such potential multi-level mode of action of diltiazem.

575

576 **Conclusions**

577 Overall, the results presented here set a solid baseline for our drug repurposing strategy and for
578 the use of diltiazem as a host-targeted antiviral in clinical practice. Moreover, the increased
579 antiviral efficacy observed in reconstituted human airway epithelium (**Figures 5B and S6 Table**)
580 plead in favor of the combination of diltiazem with the virus-targeted antiviral oseltamivir for the
581 improvement of current anti-influenza therapy, and possibly decreasing the risk of development
582 of viral resistance. In that regard, our results prompted a French multicenter randomized clinical
583 trial aimed at assessing the effect of diltiazem-oseltamivir bitherapy compared with standard
584 oseltamivir monotherapy for the treatment of severe influenza infections in intensive care units,
585 hence completing the bedside-to-bench and bench-to-bedside cycle of our innovative approach.
586 Additionally, retrospective signature analysis of sequential respiratory samples from patients

587 included in both study arms and stratified according to their clinical response to treatment will
588 provide valuable data to pursue the investigations on the specific mediators of the diltiazem-
589 related antiviral response. This trial (FLUNEXT TRIAL PHRC #15-0442, ClinicalTrials.gov
590 identifier NCT03212716) is currently ongoing.

591 Finally, our study underscores the high value of clinical specimens and the advantages of
592 exploiting virogenomic and chemogenomic data for the successful systematic repurposing of
593 drugs already available in our modern pharmacopeia as new effective antivirals. We propose that
594 our approach targeting respiratory epithelial cells, the principal influenza infected cell type in the
595 lung, could be extended to other respiratory viruses and eventually to other pathogens involved
596 in acute infections. Importantly, drug repurposing presents several financial and regulatory
597 advantages compared to the development of *de novo* molecules [5], which are of particular
598 interest not only in the context of antimicrobial resistance but also against both emerging or
599 recurrent pathogens for which we are still disarmed.

600

601 **Declarations**

602

603 **Ethics approval and consent to participate:** Adult patients were recruited by general
604 practitioners in the context of a previously published randomized clinical trial (Escuret et al.,
605 2012) (ClinicalTrials.gov identifier NCT00830323) and all of them provided written informed
606 consent. The study protocol was approved by the Lyon Ethics Committee (Comité de Protection
607 des Personnes Lyon B) on September 9th, 2009 and conducted in accordance with the
608 Declaration of Helsinki.

609 All animal procedures were approved by the Institutional Animal Care Committee of the Centre
610 Hospitalier Universitaire de Québec (CPAC protocol authorization #2012-068-3) according to
611 the guidelines of the Canadian Council on Animal Care.

612 **Consent for publication:** Not applicable.

613 **Availability of data and material:** The main datasets supporting the conclusions of this article
614 are included within the article and its additional files. All raw microarray data from virogenomic
615 signatures were deposited on the National Center for Biotechnology Information's Gene
616 Expression Omnibus (GEO), under accession number GSE93731. Other datasets used and/or
617 analyzed during the current study are available from the corresponding authors on reasonable
618 request.

619 **Competing interests:** AP, OT, JT, GB and MRC are co-inventors of a patent application filed by
620 INSERM, Université Claude Bernard Lyon 1, Laval University and Hospices Civils de Lyon for
621 the repurposing of diltiazem and etilefrine as anti-influenza agents (FR15/52284 -
622 PCT/ep2016/056036 - WO2016146836). The authors have no additional financial interests.

623 **Funding:** This work was funded by grants from the French Ministry of Social Affairs and Health
624 (DGOS), Institut National de la Santé et de la Recherche Médicale (INSERM), the Université
625 Claude Bernard Lyon 1, the Région Auvergne Rhône-Alpes (CMIRA N° 14007029 and
626 AccueilPro COOPERA N°15458 grants), and Canadian Institutes of Health Research (N°
627 229733 and 230187). Guy Boivin is the holder of the Canada Research Chair on influenza and
628 other respiratory viruses. Funding institutions had no participation in the design of the study,
629 collection, analysis and interpretation of data, or in the writing of the manuscript.

630 **Authors' contributions:** AP, OT, JT, GB and MRC designed and coordinated the study. VE, JP
631 and BL acquired clinical data from the cohort. AP, OT, TJ, BP, AT, MR, MEH, CR, CNL, SC,
632 CLL and JT performed experiments and provided technical support. AP, OT, MR, JP, JT, GB
633 and MRC interpreted data. AP, OT and MRC wrote the manuscript. JT, GB and MRC revised
634 the manuscript.

635 **Acknowledgements:** The authors want to thank Jacques Corbeil and Frederic Raymond
636 (Research Center in Infectious Diseases of the CHU de Quebec and Laval University, Quebec)
637 for their help and useful advice.

638

639 **References**

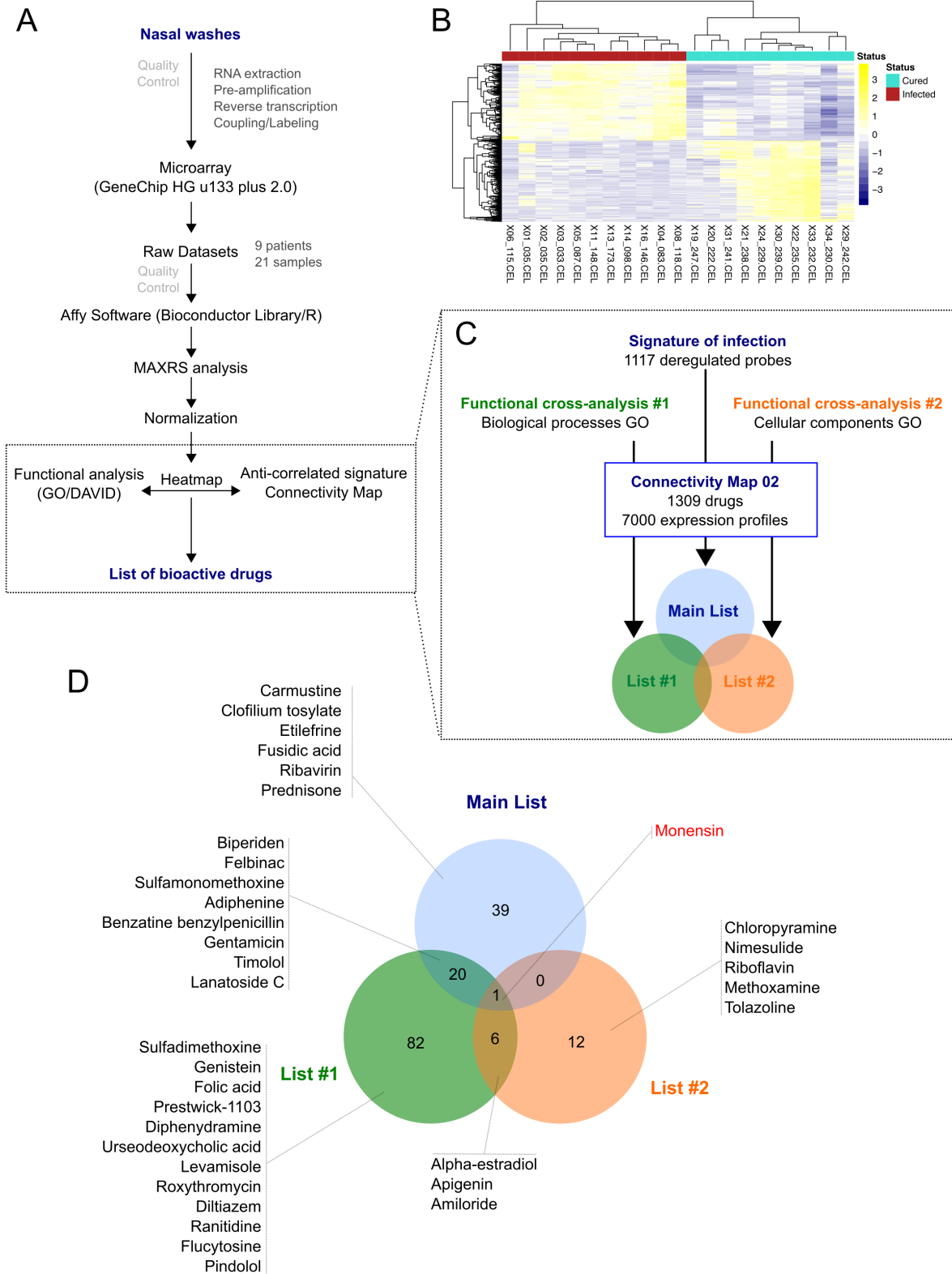
- 640 1. Influenza facts Sheet n°211. 2014. <http://www.who.int/mediacentre/factsheets/fs211/en/>.
641 Accessed 20 Jan 2016.
- 642 2. Loregian A, Mercorelli B, Nannetti G, Compagnin C, Palù G. Antiviral strategies against
643 influenza virus: towards new therapeutic approaches. *Cell Mol Life Sci CMLS*. 2014;71:3659–
644 83.
- 645 3. Booth B, Zimmel R. Prospects for productivity. *Nat Rev Drug Discov*. 2004;3:451–6.
- 646 4. Ashburn TT, Thor KB. Drug repositioning: identifying and developing new uses for existing
647 drugs. *Nat Rev Drug Discov*. 2004;3:673–83.
- 648 5. Law GL, Tisoncik-Go J, Korth MJ, Katze MG. Drug repurposing: a better approach for
649 infectious disease drug discovery? *Curr Opin Immunol*. 2013;25:588–92.
- 650 6. Johansen LM, DeWald LE, Shoemaker CJ, Hoffstrom BG, Lear-Rooney CM, Stossel A, et al.
651 A screen of approved drugs and molecular probes identifies therapeutics with anti-Ebola virus
652 activity. *Sci Transl Med*. 2015;7:290ra89.
- 653 7. Xu M, Lee EM, Wen Z, Cheng Y, Huang W-K, Qian X, et al. Identification of small-molecule
654 inhibitors of Zika virus infection and induced neural cell death via a drug repurposing screen.
655 *Nat Med*. 2016;22:1101–7.
- 656 8. Naylor S, Schonfeld JM. Therapeutic drug repurposing, repositioning and rescue - Part I:
657 Overview. *Drug Discov World*. 2014;16.
658 https://www.researchgate.net/publication/286670692_Therapeutic_drug_repurposing_repositioning_and_rescue_-_Part_I_Overview. Accessed 11 Jan 2017.
659
- 660 9. Keiser MJ, Setola V, Irwin JJ, Laggner C, Abbas AI, Hufeisen SJ, et al. Predicting new
661 molecular targets for known drugs. *Nature*. 2009;462:175–81.
- 662 10. Haupt VJ, Schroeder M. Old friends in new guise: repositioning of known drugs with
663 structural bioinformatics. *Brief Bioinform*. 2011;12:312–26.
- 664 11. Li Y, Agarwal P. A pathway-based view of human diseases and disease relationships. *PLoS*
665 *One*. 2009;4:e4346.
- 666 12. Lussier YA, Chen JL. The emergence of genome-based drug repositioning. *Sci Transl Med*.
667 2011;3:96ps35.
- 668 13. Hütter G, Bodor J, Ledger S, Boyd M, Millington M, Tsie M, et al. CCR5 Targeted Cell
669 Therapy for HIV and Prevention of Viral Escape. *Viruses*. 2015;7:4186–203.
- 670 14. Ludwig S. Disruption of virus-host cell interactions and cell signaling pathways as an anti-
671 viral approach against influenza virus infections. *Biol Chem*. 2011;392:837–47.

- 672 15. Rossignol JF, La Frazia S, Chiappa L, Ciucci A, Santoro MG. Thiazolidines, a new class of
673 anti-influenza molecules targeting viral hemagglutinin at the post-translational level. *J Biol*
674 *Chem.* 2009;284:29798–808.
- 675 16. Belser JA, Lu X, Szretter KJ, Jin X, Aschenbrenner LM, Lee A, et al. DAS181, a novel
676 sialidase fusion protein, protects mice from lethal avian influenza H5N1 virus infection. *J Infect*
677 *Dis.* 2007;196:1493–9.
- 678 17. Mazur I, Wurzer WJ, Ehrhardt C, Pleschka S, Puthavathana P, Silberzahn T, et al.
679 Acetylsalicylic acid (ASA) blocks influenza virus propagation via its NF-kappaB-inhibiting
680 activity. *Cell Microbiol.* 2007;9:1683–94.
- 681 18. Josset L, Textoris J, Loriod B, Ferraris O, Moules V, Lina B, et al. Gene expression
682 signature-based screening identifies new broadly effective influenza a antivirals. *PloS One.*
683 2010;5.
- 684 19. Lamb J, Crawford ED, Peck D, Modell JW, Blat IC, Wrobel MJ, et al. The Connectivity
685 Map: using gene-expression signatures to connect small molecules, genes, and disease. *Science.*
686 2006;313:1929–35.
- 687 20. Lamb J. The Connectivity Map: a new tool for biomedical research. *Nat Rev Cancer.*
688 2007;7:54–60.
- 689 21. Escuret V, Cornu C, Boutitie F, Enouf V, Mosnier A, Bouscambert-Duchamp M, et al.
690 Oseltamivir-zanamivir bitherapy compared to oseltamivir monotherapy in the treatment of
691 pandemic 2009 influenza A(H1N1) virus infections. *Antiviral Res.* 2012;96:130–7.
- 692 22. Khaznadar Z, Boissel N, Agaugué S, Henry G, Cheok M, Vignon M, et al. Defective NK
693 Cells in Acute Myeloid Leukemia Patients at Diagnosis Are Associated with Blast
694 Transcriptional Signatures of Immune Evasion. *J Immunol Baltim Md 1950.* 2015;195:2580–90.
- 695 23. Degletagne C, Keime C, Rey B, de Dinechin M, Forcheron F, Chuchana P, et al.
696 Transcriptome analysis in non-model species: a new method for the analysis of heterologous
697 hybridization on microarrays. *BMC Genomics.* 2010;11:344.
- 698 24. Tukey J, Wilder J. *Exploratory Data Analysis.* Addison-Wesley; 1977.
- 699 25. Benjamini Y, Hochberg Y. Controlling the False Discovery Rate: A Practical and Powerful
700 Approach to Multiple Testing. *J R Stat Soc Ser B Methodol.* 1995;57:289–300.
- 701 26. Barrett T, Edgar R. Gene expression omnibus: microarray data storage, submission, retrieval,
702 and analysis. *Methods Enzymol.* 2006;411:352–69.
- 703 27. Dennis G Jr, Sherman BT, Hosack DA, Yang J, Gao W, Lane HC, et al. DAVID: Database
704 for Annotation, Visualization, and Integrated Discovery. *Genome Biol.* 2003;4:P3.
- 705 28. Ashburner M, Ball CA, Blake JA, Botstein D, Butler H, Cherry JM, et al. Gene ontology:
706 tool for the unification of biology. The Gene Ontology Consortium. *Nat Genet.* 2000;25:25–9.

- 707 29. Hatakeyama S, Sakai-Tagawa Y, Kiso M, Goto H, Kawakami C, Mitamura K, et al.
708 Enhanced expression of an alpha2,6-linked sialic acid on MDCK cells improves isolation of
709 human influenza viruses and evaluation of their sensitivity to a neuraminidase inhibitor. *J Clin*
710 *Microbiol.* 2005;43:4139–46.
- 711 30. Moules V, Ferraris O, Terrier O, Giudice E, Yver M, Rolland JP, et al. In vitro
712 characterization of naturally occurring influenza H3NA- viruses lacking the NA gene segment:
713 toward a new mechanism of viral resistance? *Virology.* 2010;404:215–24.
- 714 31. Tsai AW, McNeil CF, Leeman JR, Bennett HB, Nti-Addae K, Huang C, et al. Novel Ranking
715 System for Identifying Efficacious Anti-Influenza Virus PB2 Inhibitors. *Antimicrob Agents*
716 *Chemother.* 2015;59:6007–16.
- 717 32. Bolger AM, Lohse M, Usadel B. Trimmomatic: a flexible trimmer for Illumina sequence
718 data. *Bioinforma Oxf Engl.* 2014;30:2114–20.
- 719 33. Bray NL, Pimentel H, Melsted P, Pachter L. Near-optimal probabilistic RNA-seq
720 quantification. *Nat Biotechnol.* 2016;34:525–7.
- 721 34. Robinson MD, McCarthy DJ, Smyth GK. edgeR: a Bioconductor package for differential
722 expression analysis of digital gene expression data. *Bioinforma Oxf Engl.* 2010;26:139–40.
- 723 35. Dupinay T, Nguyen A, Croze S, Barbet F, Rey C, Mavingui P, et al. Next-generation
724 sequencing of ultra-low copy samples: From clinical FFPE samples to single-cell sequencing.
725 *Curr Top Virol.* 2013;10:63–83.
- 726 36. Kinsella RJ, Kähäri A, Haider S, Zamora J, Proctor G, Spudich G, et al. Ensembl BioMarts: a
727 hub for data retrieval across taxonomic space. *Database J Biol Databases Curation.*
728 2011;2011:bar030.
- 729 37. Flicek P, Amode MR, Barrell D, Beal K, Billis K, Brent S, et al. Ensembl 2014. *Nucleic*
730 *Acids Res.* 2014;42 Database issue:D749-755.
- 731 38. Durr FE, Lindh HF. Efficacy of ribavirin against influenza virus in tissue culture and in mice.
732 *Ann N Y Acad Sci.* 1975;255:366–71.
- 733 39. Leyssen P, De Clercq E, Neyts J. Molecular strategies to inhibit the replication of RNA
734 viruses. *Antiviral Res.* 2008;78:9–25.
- 735 40. Alonso FV, Compans RW. Differential effect of monensin on enveloped viruses that form at
736 distinct plasma membrane domains. *J Cell Biol.* 1981;89:700–5.
- 737 41. Hayden F. Developing new antiviral agents for influenza treatment: what does the future
738 hold? *Clin Infect Dis Off Publ Infect Dis Soc Am.* 2009;48 Suppl 1:S3-13.
- 739 42. Lee SM-Y, Yen H-L. Targeting the host or the virus: current and novel concepts for antiviral
740 approaches against influenza virus infection. *Antiviral Res.* 2012;96:391–404.

- 741 43. Koh Y. Update in acute respiratory distress syndrome. *J Intensive Care*. 2014;2:2.
- 742 44. Poissy J, Terrier O, Lina B, Textoris J, Rosa-Calatrava M. La modulation de la signature
743 transcriptomique de l'hôte infecté : une nouvelle stratégie thérapeutique dans les viroses graves ?
744 Exemple de la grippe. *Réanimation*. 2016;25:53–61.
- 745 45. Lou Z, Sun Y, Rao Z. Current progress in antiviral strategies. *Trends Pharmacol Sci*.
746 2014;35:86–102.
- 747 46. Dayekh K, Johnson-Obaseki S, Corsten M, Villeneuve PJ, Sekhon HS, Weberpals JI, et al.
748 Monensin inhibits epidermal growth factor receptor trafficking and activation: synergistic
749 cytotoxicity in combination with EGFR inhibitors. *Mol Cancer Ther*. 2014;13:2559–71.
- 750 47. Zhang Y, Jamaluddin M, Wang S, Tian B, Garofalo RP, Casola A, et al. Ribavirin treatment
751 up-regulates antiviral gene expression via the interferon-stimulated response element in
752 respiratory syncytial virus-infected epithelial cells. *J Virol*. 2003;77:5933–47.
- 753 48. Pubchem C10H15NO2. Etilefrine | C10H15NO2 - PubChem.
754 <https://pubchem.ncbi.nlm.nih.gov/compound/Etilefrine>. Accessed 3 Feb 2017.
- 755 49. Pubchem C22H26N2O4S. diltiazem | C22H26N2O4S - PubChem.
756 <https://pubchem.ncbi.nlm.nih.gov/compound/diltiazem>. Accessed 3 Feb 2017.
- 757 50. Fujioka Y, Nishide S, Ose T, Suzuki T, Kato I, Fukuhara H, et al. A Sialylated Voltage-
758 Dependent Ca²⁺ Channel Binds Hemagglutinin and Mediates Influenza A Virus Entry into
759 Mammalian Cells. *Cell Host Microbe*. 2018;23:809-818.e5.

760 **27/08/2018 14:49:00**

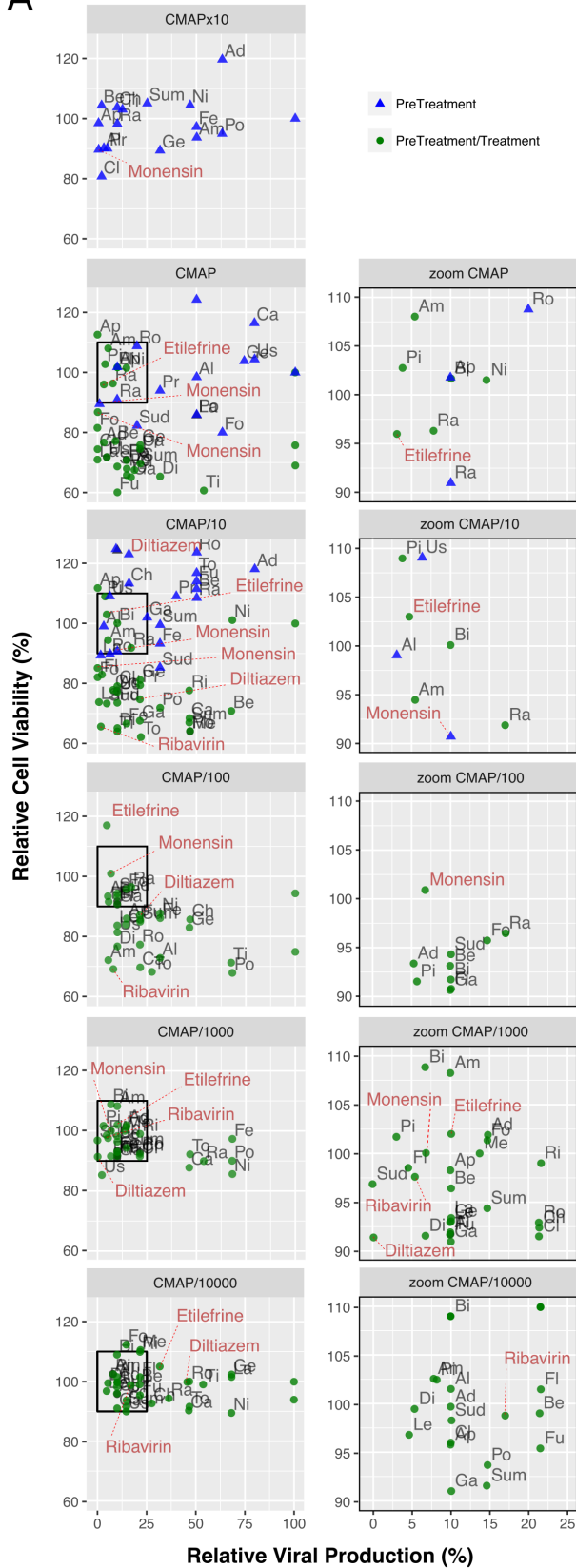


762 **Fig. 1. From nasal wash clinical samples to a shortlist of 35 candidate molecules. (A)**

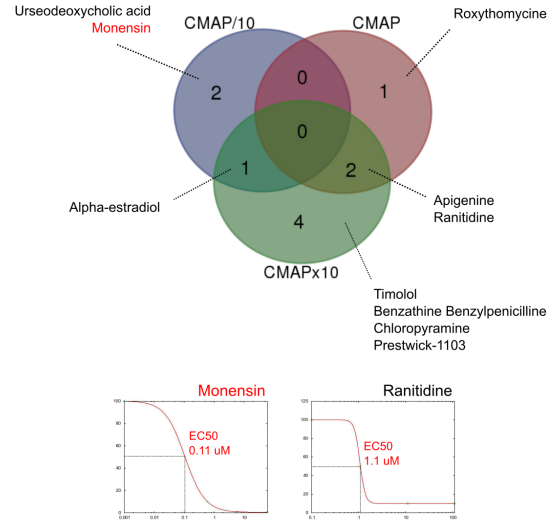
763 Overview of the *in silico* strategy used in this study. A detailed description of the strategy is
764 described in the Online Methods section. **(B)** Hierarchical clustering and heatmap of the 1,117
765 most differentially deregulated genes between “infected” (red) and “cured” (light green) samples.
766 Raw median centered expression levels are color coded from blue to yellow. Dendrograms
767 indicate the correlation between clinical samples (columns) or genes (rows). **(C)** Functional
768 cross-analysis of candidate molecules obtained from Connectivity Map (CMAP). Three lists of
769 candidate molecules were obtained using different set of genes in order to introduce functional
770 bias and add more biological significance to this first screening: a Main List based on the
771 complete list of differentially expressed genes, and two other lists (List #1 and #2) based on
772 subsets of genes belonging to significantly enriched Gene Ontology (GO) terms. **(D)** Venn
773 Diagram comparing the total 160 molecules obtained from the three lists described in (C), with
774 monensin as the only common molecule. Only the candidates selected for *in vitro* screening and
775 validation are depicted.

776

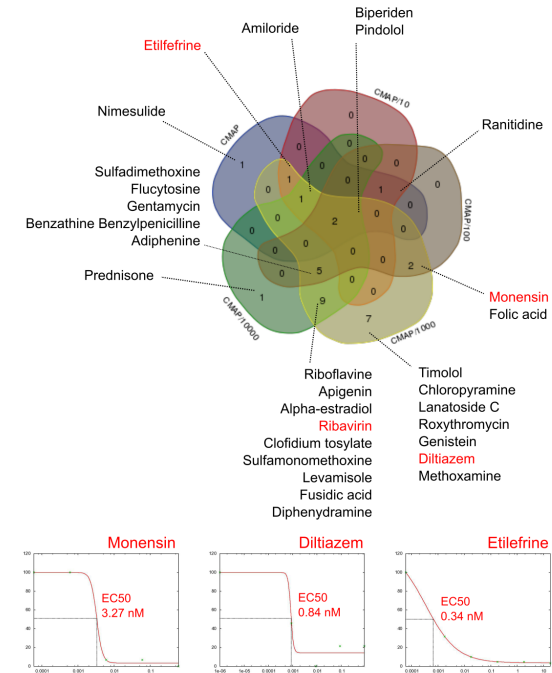
A



B



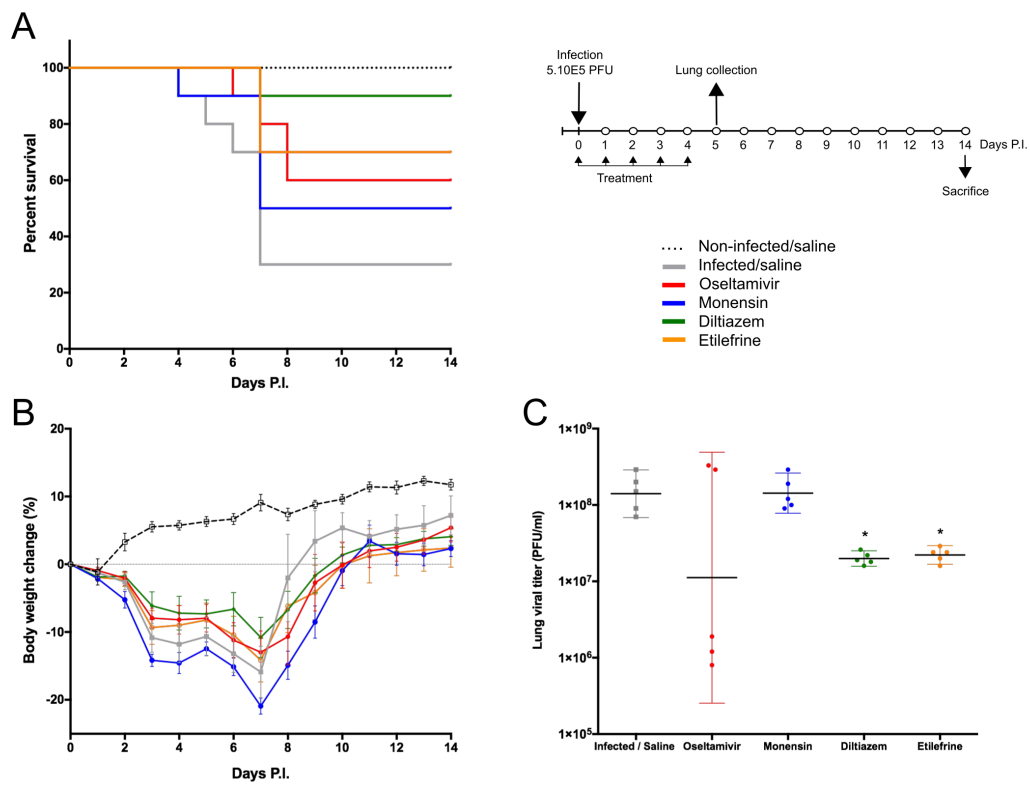
C



778 **Fig. 2. Screening and validation of the effect of selected molecules on A(H1N1)pdm09 viral**
779 **growth *in vitro*.** (A, left) Evaluation on A549 cells of the antiviral potency of the 35 candidates
780 selected by *in silico* analysis. Relative viral production (%; X axis) and relative cell viability (%;
781 Y axis) of both pre-treatment (blue triangles) and pre-treatment/treatment (green circles)
782 regimens were evaluated. A 10-fold drug concentration range using CMAP as reference (CMAP
783 x10, CMAP, CMAP/10, CMAP/100, CMAP/1,000 and CMAP/10,000) was used. CMAPx10
784 was only tested in the context of pre-treatment, by anticipation of a lower efficacy of molecules
785 in this experimental setup. All experimental assays were performed in triplicate and mean values
786 are represented. (A, right) Zoom panels depicting molecules defined as “inhibitors” according to
787 the following two criteria: i) induce a 75% or higher reduction on viral production, and ii) have
788 minor impact on cell viability, with relative values in the 90%-110% range. For clarity purposes,
789 with the exception of diltiazem, etilefrine, monensin and ribavirin, abbreviations were used:
790 Adiphenine "Ad"; Alpha-estradiol "Al"; Amiloride "Am"; Apigenin "Ap"; Benzathine
791 Benzylpenicilline "Be"; Biperiden "Bi"; Carmustine "Ca"; Chloropyramine "Ch"; Clofidium
792 tosylate "Cl"; Diphenhydramine "Di"; Felbinac "Fe"; Flucytosine "Fl"; Folic acid "Fo"; Fusidic
793 acid "Fu"; Genistein "Ge"; Gentamycin "Ga"; Lanatoside C "La"; Levamisole "Le";
794 Methoxamine "Me"; Nimesulide "Ni"; Pindolol "Pi"; Prednisone "Po"; Prestwick-1103 "Pr";
795 Ranitidine "Ra"; Riboflavine "Ri"; Roxythromycin "Ro"; Sulfadimethoxine "Sud";
796 Sulfamonomethoxine "Sum"; Timolol "Ti"; Tolazoline "To"; Urseodeoxycholic acid "Us".
797 Dose-response curves for all the 35 molecules are presented in Supplementary Table 3. (B) Venn
798 diagram of the 10 molecules identified in pre-treatment (10/35; 28.57%) and matching the
799 “inhibitor” criteria, mainly when used at 10-fold CMAP concentration. EC50 curves for
800 monensin and ranitidine are represented. (C) Venn diagram of the 30 “inhibitor” molecules

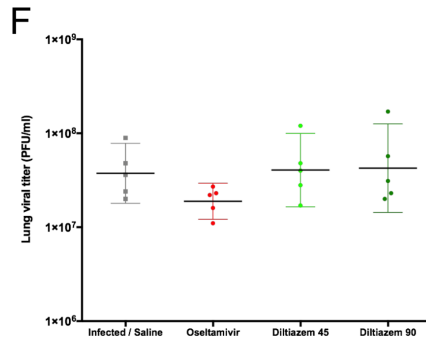
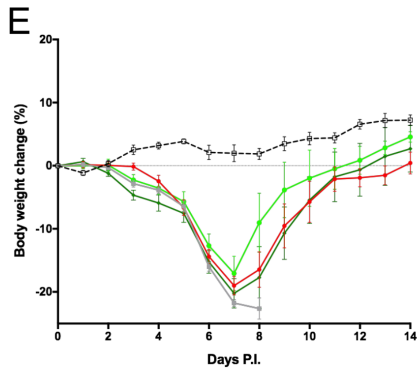
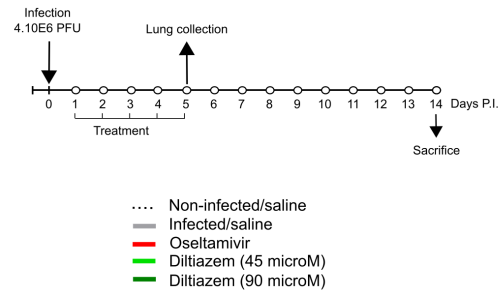
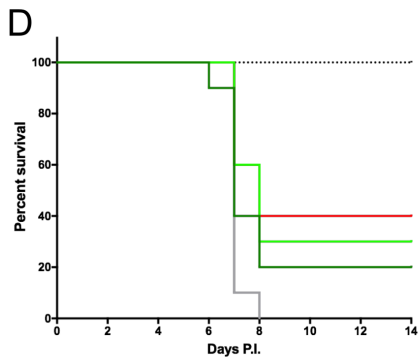
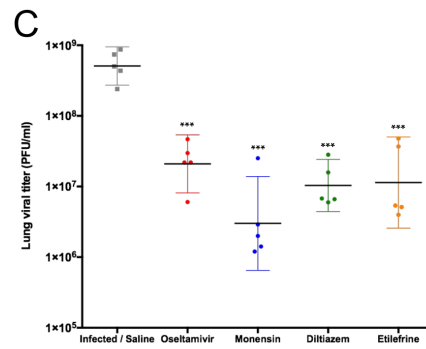
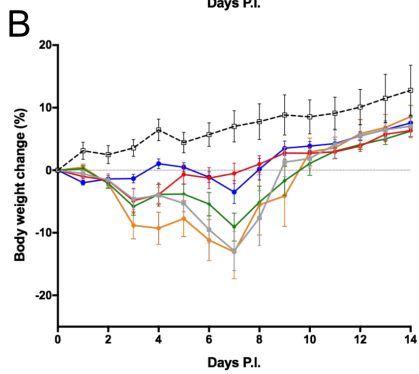
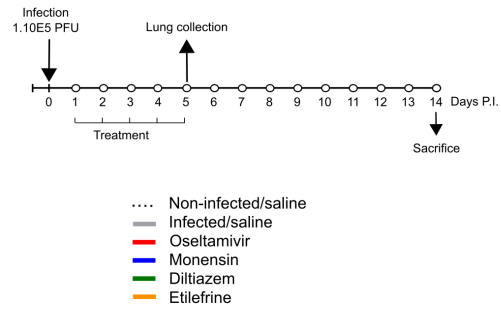
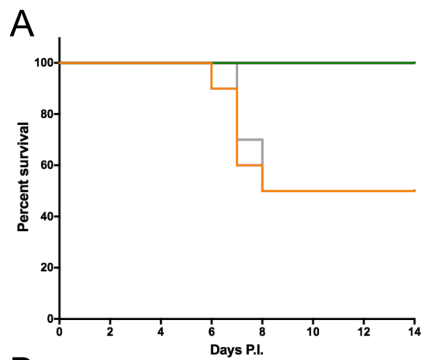
801 identified in pre-treatment/treatment (30/35; 85.7%). EC50 curves for monensin, diltiazem and
802 etilefrine are represented.

803



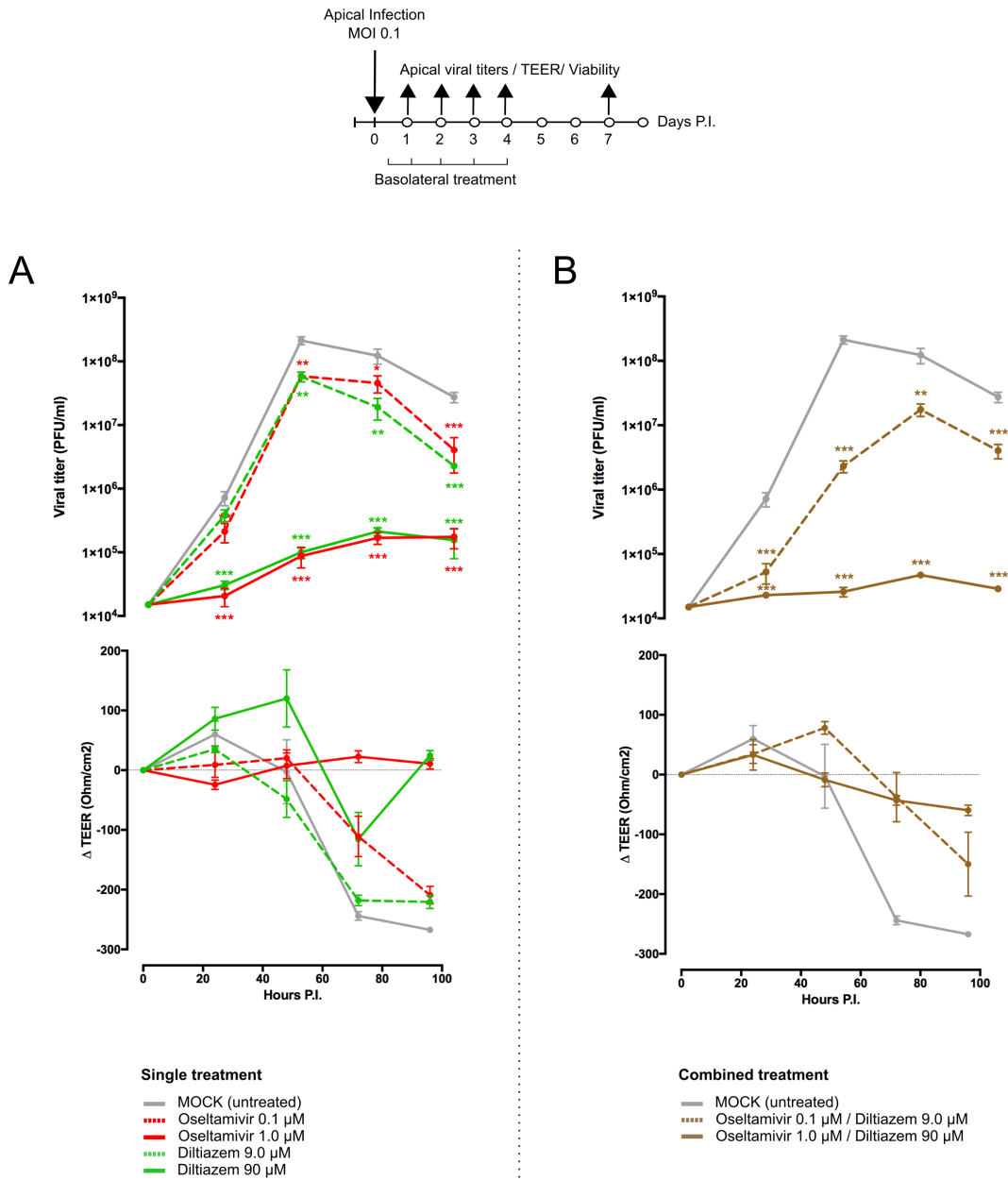
805 **Fig. 3. Efficacy of oral administration of selected molecules in mice infected with influenza**
806 **A(H1N1)pdm09 virus.** C57BL/6N mice (n=15/group) were intranasally inoculated with 5×10^5
807 PFU of influenza A/Quebec/144147/09 virus on day 0 and treated by gavage with saline (grey),
808 oseltamivir 10 mg/kg/day (red), monensin 10 mg/kg/day (blue), diltiazem 90 mg/kg/day (green),
809 or etilefrine 3 mg/kg/day (orange). A mock-infected, saline-treated group (black dotted line, n=6)
810 was included as control. Treatments were initiated on day 0 (6 h before infection) and
811 administered once daily for 5 consecutive days. **(A)** Survival rates (n=10/group), **(B)** mean
812 weight changes (\pm SEM, n=10/group or remaining mice) and **(C)** median (\pm CI95, n=5/group)
813 lung viral titers on day 5 p.i. are shown. *p<0.05, **p<0.01 and ***p<0.001 compared to the
814 infected saline-treated group by one-way ANOVA with Tukey's post-test. Data are
815 representative of two independent experiments.

816



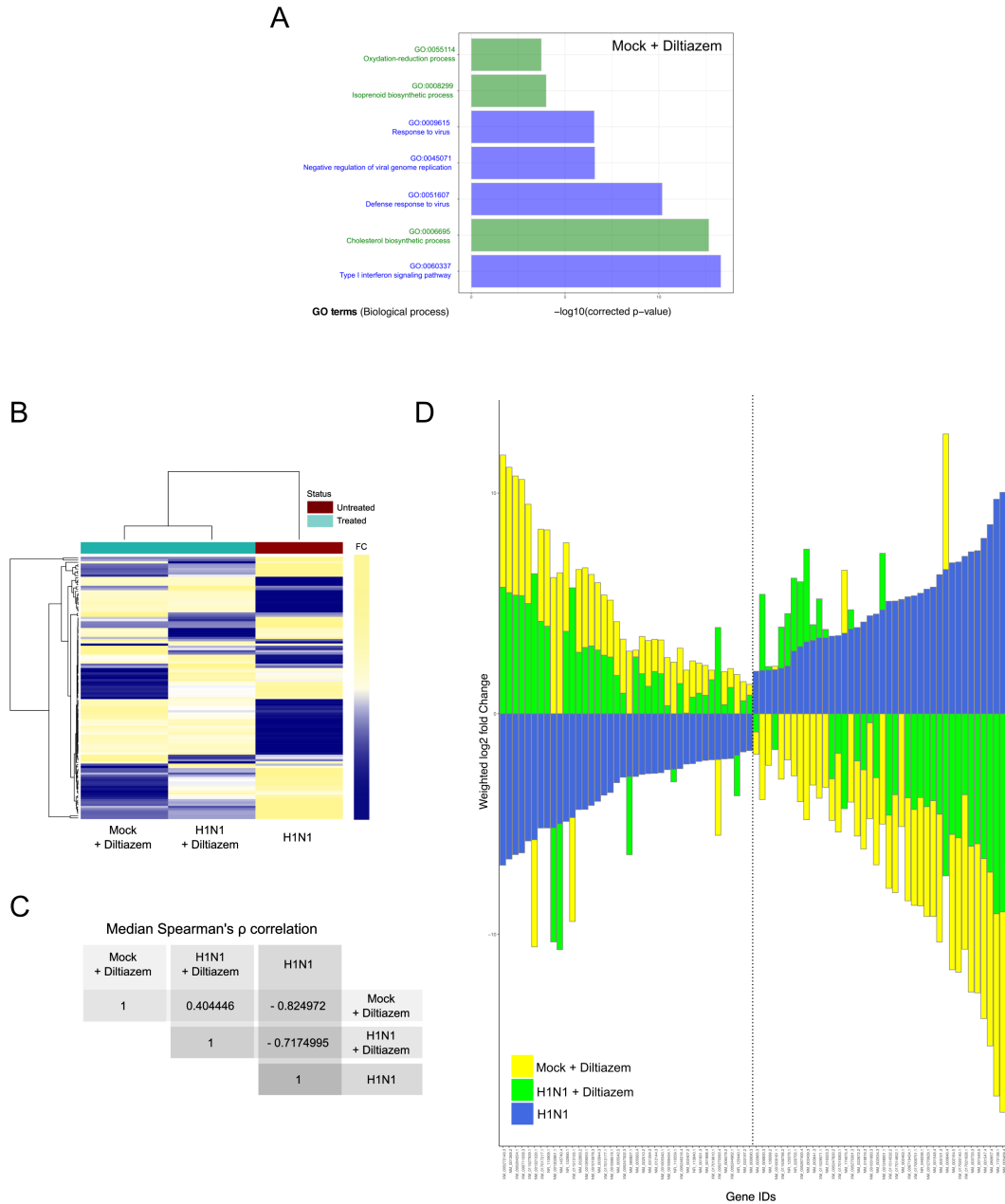
818 **Fig. 4. Efficacy of post-infection oral treatment with diltiazem and etilefrine in mice**
819 **infected with influenza A(H1N1)pdm09 virus.** C57BL/6N mice (n=15/group) were
820 intranasally inoculated with 1×10^5 (A-C) or 4×10^6 (D-F) PFU of influenza
821 A/Quebec/144147/09 virus on day 0 and treated by gavage with saline (grey), oseltamivir 10
822 mg/kg/day (red), monensin 10 mg/kg/day (blue, A only), diltiazem 45 mg/kg/day (light green, B
823 only), diltiazem 90 mg/kg/day (dark green), or etilefrine 3 mg/kg/day (orange, A only). A mock-
824 infected, saline-treated group (black dotted line, n=6) was included as control. Treatments were
825 initiated on day 1 (24 h after infection and administered once daily for 5 consecutive days. (A,
826 D) Survival rates (n=10/group), (B, E) mean weight changes (\pm SEM, n=10/group or remaining
827 mice), and (C, F) median (\pm CI95, n=5/group) lung viral titers on day 5 p.i. are shown. *p<0.05,
828 **p<0.01 and ***p<0.001 compared to the infected saline-treated group by one-way ANOVA
829 with Tukey's post-test. Data are representative of two independent experiments.

830



832 **Fig. 5. Diltiazem significantly reduces viral replication in infected reconstituted human**
833 **airway epithelia (HAE).** Apical viral production (\pm SEM) and transepithelial electrical
834 resistance (Δ TEER \pm SEM) in MucilAir® human airway epithelium infected on the apical pole
835 with influenza A/Lyon/969/09 (H1N1)pdm09 virus at a MOI of 0.1 and subjected to **(A)** single
836 or **(B)** combined treatments by the basolateral pole. Treatments with culture medium (mock,
837 grey), oseltamivir 0.1 μ M (red, dotted line), oseltamivir 1 μ M (red, solid line), diltiazem 9 μ M
838 (green, dotted line), diltiazem 90 μ M (green, solid line), oseltamivir 0.1 μ M / diltiazem 9 μ M
839 (brown, dotted line) or oseltamivir 1 μ M / diltiazem 90 μ M (brown, solid line) were initiated 5 h
840 after infection and administered once daily for 5 consecutive days. * p <0.05, ** p <0.01 and
841 *** p <0.001 compared to the infected mock-treated group by one-way ANOVA with Tukey's
842 post-test. Data are representative of three independent experiments.

843



845 **Figure 6. Diltiazem treatment effectively induces significant reversion of the viral infection**
846 **signature. (A)** DAVID gene enrichment analysis of the diltiazem transcriptional signature. The
847 seven most significant biological processes (BP) are presented. BP related to antiviral response
848 and cholesterol biosynthesis/metabolism are represented in blue and green, respectively. **(B)**
849 Hierarchical clustering and heatmap of the 118 common differentially expressed transcripts
850 (absolute fold change >2, Benjamini-Hochberg corrected p-value <0.05) between mock-infected
851 / diltiazem (“mock + diltiazem”), infected / mock-treated (“H1N1”), or infected / diltiazem
852 (“H1N1 + diltiazem”) HAE. The mock-infected / mock-treated (“mock”) condition was used as
853 baseline. Mean-weighted fold changes are color-coded from blue to yellow. **(C)** Median
854 Spearman ρ correlation value calculations between the 3 conditions highlighted in the heatmap.
855 **(D)** Stacked barplot representation of the 40 most up/down-regulated transcripts highlighted in
856 the analysis. Barplots were constructed in R3.3.1 based on mean-weighted fold changes and
857 ordered according to H1N1 values (blue). Mock + diltiazem and H1N1 + diltiazem conditions
858 are represented in yellow and green, respectively.

859

860 **Table 1. Shortlist of the 35 selected molecules and their documented pharmacological**
861 **classes.** Shortlist of the 35 selected candidates representative of the 110 molecules obtained from
862 the *in silico* screening (Fig 1 and S1). Documented pharmacological classes were obtained from
863 PubChem (<https://pubchem.ncbi.nlm.nih.gov>). Asterisks (*) indicate molecules previously
864 evaluated for their antiviral properties according to the literature, and numerals (#) those
865 belonging to anti-microbial or anti-inflammatory related pharmacological classes

Table 1.

Name	Pharmacological Class
Adiphenine	Parasympatholytics/Anticholinergics/Antispasmodics
Alpha-estradiol*	5 alpha-reductase inhibitors/Androgenic alopecia treatment
Amiloride*#	Epithelial Sodium Channel Blockers/Diuretics/Acid Sensing Ion Channel Blockers
Apigenin*#	Anti-Inflammatory Agents, Non-Steroidal/?
Benzathine benzylpenicillin#	Anti-Bacterial Agents
Biperiden*	Antiparkinson Agents/Muscarinic Antagonists/Parasympatholytics
Carmustine	Antineoplastic Agents, Alkylating
Chloropyramine	Histamine H1 Antagonists
Clofilium tosylate	Anti-Arrhythmia Agents
Diltiazem	Antihypertensive Agents/Calcium Channel Blockers/Cardiovascular Agents/Vasodilator Agents
Diphenhydramine	Anesthetics, Local/Anti-Allergic Agents/Antiemetics/Histamine H1 Antagonists/Hypnotics and Sedatives
Etilefrine	Adrenergic beta-1 and alpha agonist /Cardiotonic/antihypotensive agent.
Felbinac#	Anti-Inflammatory Agents, Non-Steroidal
Flucytosine*#	Antifungal Agents/Antimetabolites
Folic acid	Hematinics/Vitamin B Complex
Fusidic acid#	Anti-Bacterial Agents/Protein Synthesis Inhibitors
Genistein	Anticarcinogenic Agents/Phytoestrogens/Protein Kinase Inhibitors
Gentamicin#	Anti-Bacterial Agents/Protein Synthesis Inhibitors
Lanatoside C	Anti-Arrhythmia Agents
Levamisole*	Adjuvants, Immunologic/Antinematodal Agents/Antirheumatic Agents
Methoxamine	Adrenergic alpha-1 Receptor Agonists/Sympathomimetics/Vasoconstrictor Agents
Monensin*#	Antifungal Agents/Antiprotozoal Agents/Coccidiostats/Proton Ionophores/Sodium Ionophores
Nimesulide*#	Anti-Inflammatory Agents, Non-Steroidal/Cyclooxygenase Inhibitors
Pindolol	Adrenergic beta-Antagonists/Antihypertensive Agents/Serotonin Antagonists/Vasodilator Agents
Prednisone#	Anti-Inflammatory Agents/Antineoplastic Agents, Hormonal/Glucocorticoids
Prestwick-1103#	Anti-Inflammatory Agents, Non-Steroidal/Cyclooxygenase Inhibitors
Ranitidine	Anti-Ulcer Agents/Histamine H2 Antagonists
Ribavirin*	Antimetabolites/Antiviral Agents
Riboflavin*	Photosensitizing Agents/Vitamin B Complex
Roxithromycin#	Anti-Bacterial Agents
Sulfadimethoxine#	Anti-Infective Agents
Sulfamonomethoxine#	Anti-Infective Agents
Timolol*	Adrenergic beta-Antagonists/Anti-Arrhythmia Agents/Antihypertensive Agents
Tolazoline	Adrenergic alpha-Antagonists/Antihypertensive Agents/Vasodilator Agents
Ursodeoxycholic acid	Cholagogues and Cholaretics

Supplementary Materials

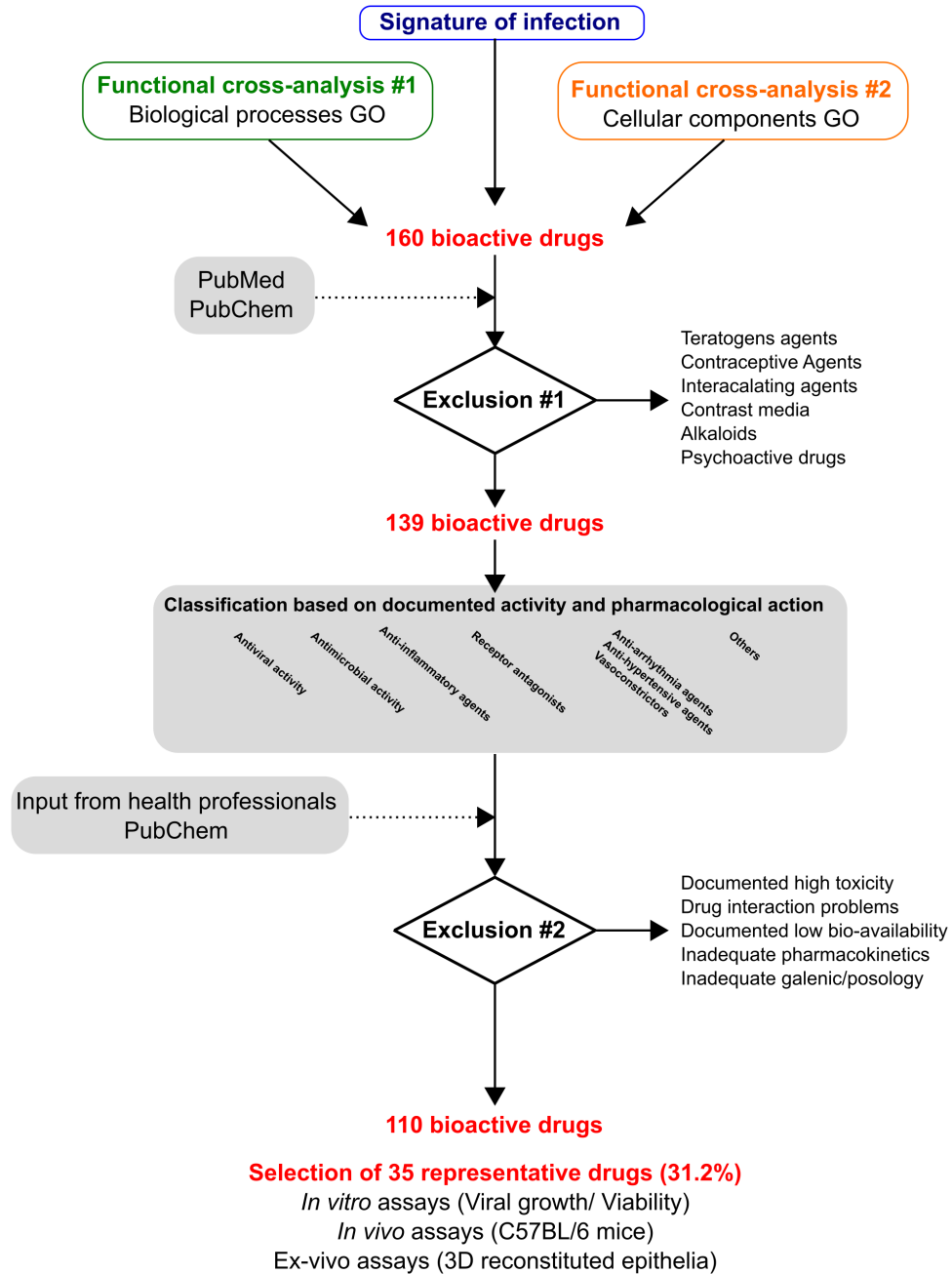


Fig. S1. Decision tree used to rationally reduce the number of drug candidates. Bioactive molecules were excluded if not compatible with a final use as antiviral, mostly for safety (e.g. teratogens, intercalating agents) and/or pharmacological (e.g. documented low bioavailability) reasons. An additional selection level based on analysis of documented pharmacological actions was included, to finally define a shortlist of 35 representative molecules (<3% of CMAP) for in vitro screening (Table 1).

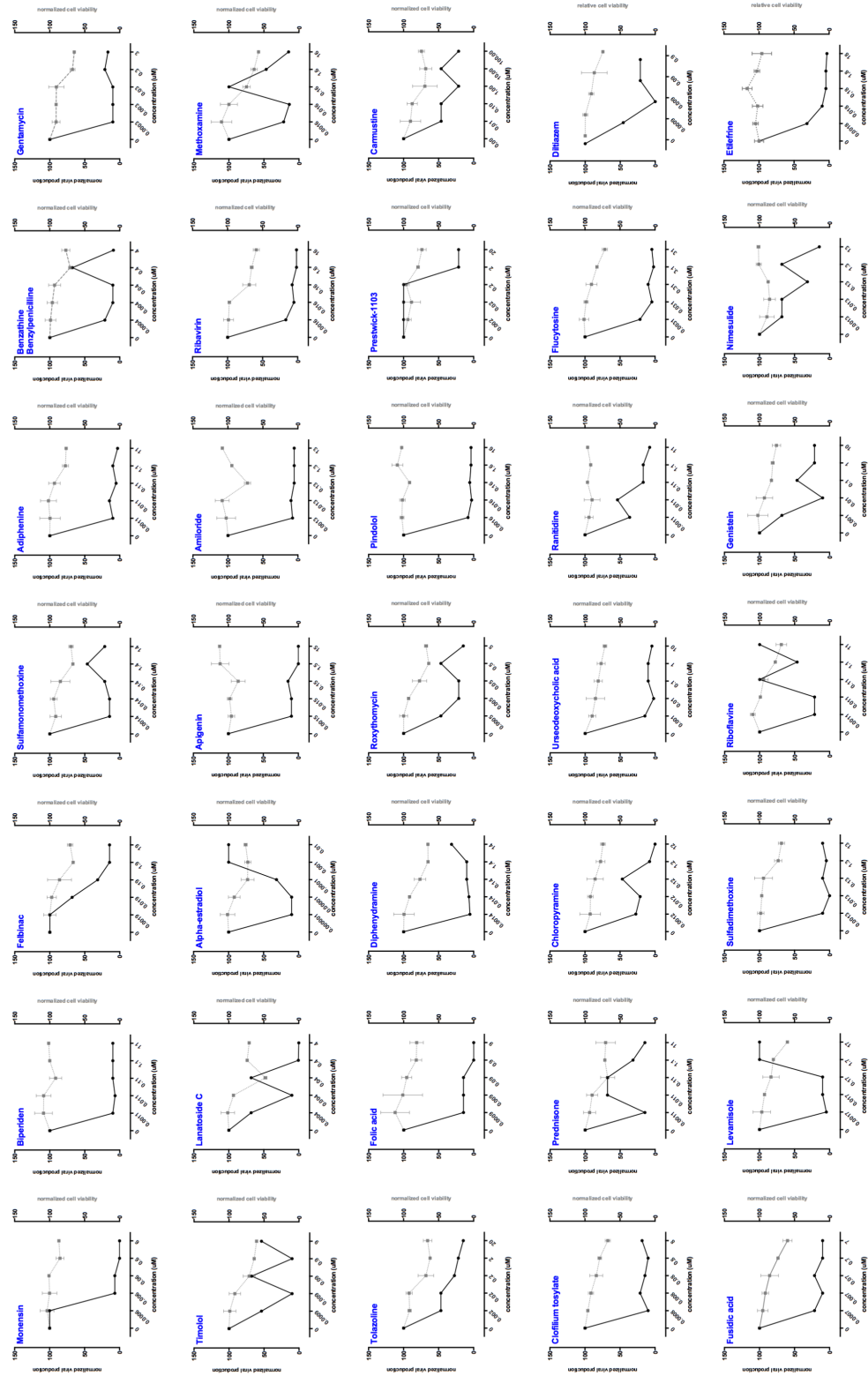
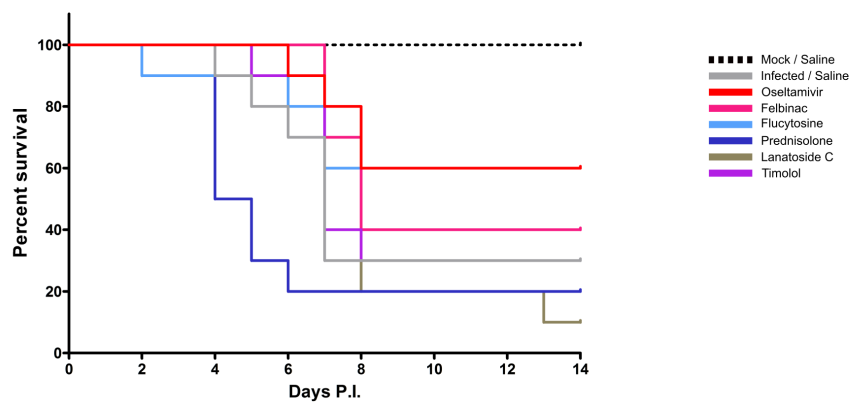


Fig. S2. Dose-response curves for the 35 molecules tested *in vitro*. In comparison with a mock-treated control, the impact of pre-treatment/treatment on % relative viral production (black line, left Y axis) and % relative cell viability (grey line, right Y axis) was measured at the indicated concentrations.

A



B

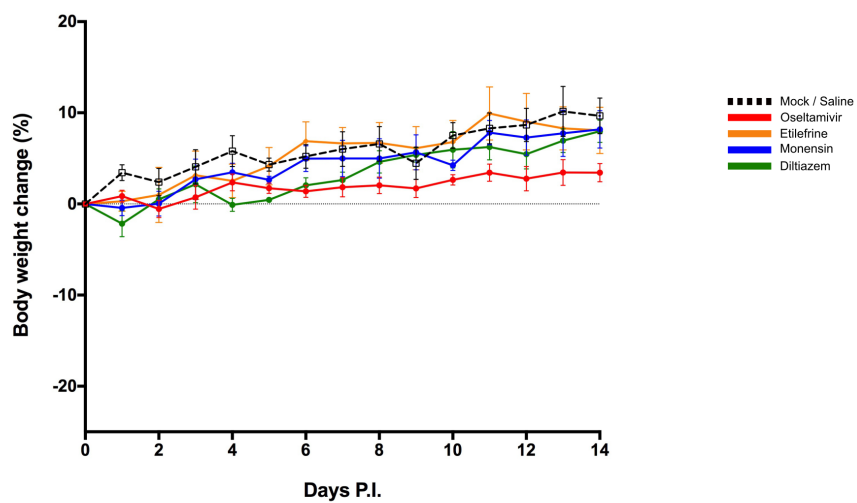


Fig. S3. Efficacy and toxicity after oral administration of selected molecules in mice. (A)

Survival curves of C57BL/6N mice (n=15/group), intranasally inoculated with 5×10^5 PFU of influenza A/Quebec/144147/09 virus on day 0 and treated by gavage with saline (grey), oseltamivir 10 mg/kg/day (red), lanatoside C 100 mg/kg/day (olive), prednisolone 5 mg/kg/day (dark blue), flucytosine 240 mg/kg/day (light blue), felbinac 5 mg/kg/day (fuchsia) or timolol 50 mg/kg/day (purple). A mock-infected, saline-treated group (black dotted line, n=6) was included as control. Treatments were initiated on day 0 (6 h before infection) and administered once daily for 5 consecutive days. (B) Body weight changes of mock-infected C57BL/6N mice (n=10/group) treated by gavage with saline (grey), oseltamivir 10 mg/kg/day (red), monensin 10 mg/kg/day (blue), diltiazem 90 mg/kg/day (green), or etilefrine 3 mg/kg/day (orange). A saline-treated group (black dotted line, n=6) was included as control. Treatments were initiated on day 0 (6 h before mock-infection) and administered once daily for 5 consecutive days.

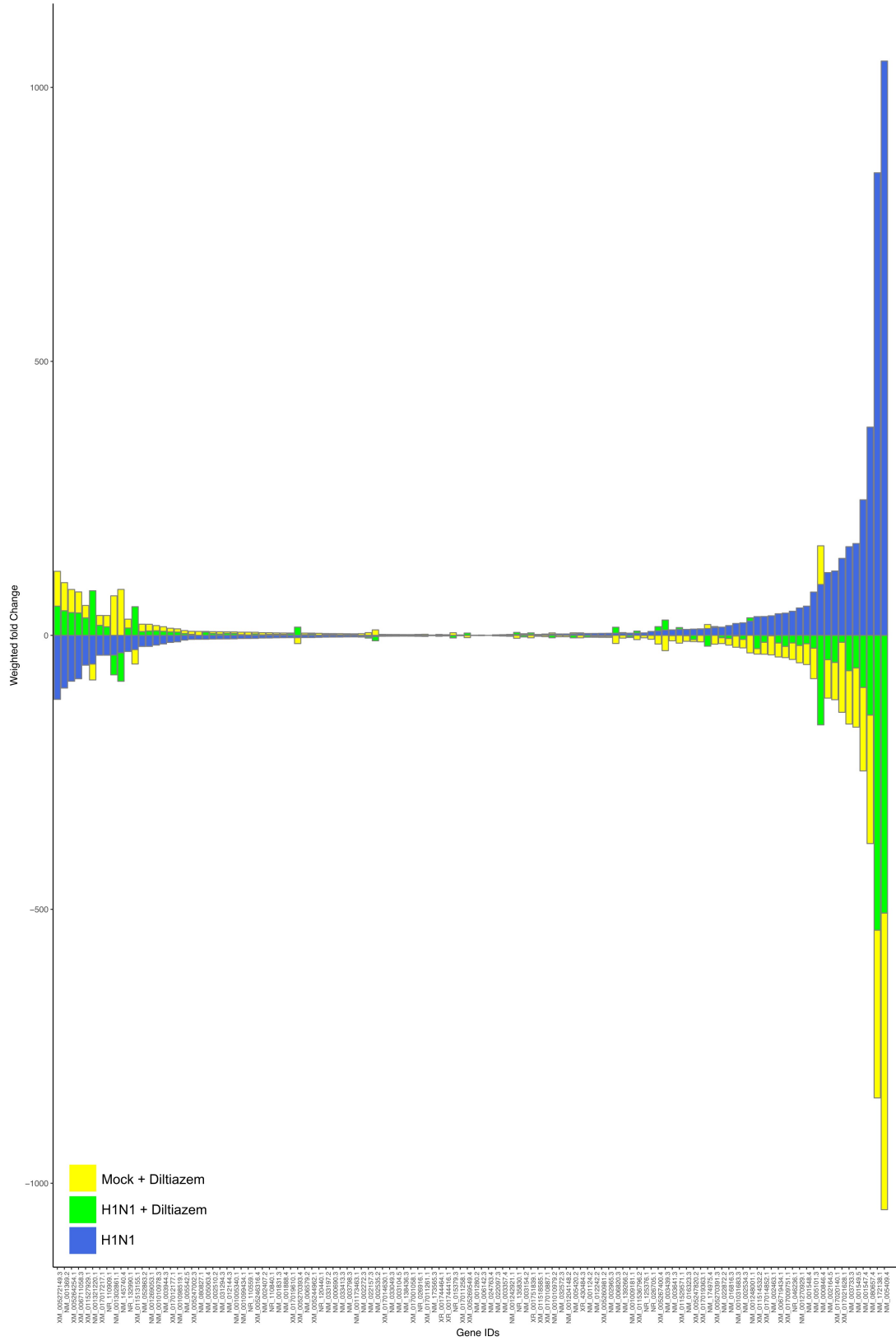


Fig. S4. Diltiazem treatment effectively induces significant reversion of the viral infection signature. Stacked barplots with mean-weighted fold changes for the complete list of the 118 common differentially expressed transcripts (absolute fold change >2 , Benjamini-Hochberg corrected p-value <0.05) between the mock + diltiazem (yellow), H1N1 (blue), and H1N1 + diltiazem (green) conditions. Barplots were constructed in R3.3.1 based on mean-weighted fold changes and ordered according to H1N1 values (blue).

Demographic Characteristics	
Number of patients	9
Male sex ratio (n,%)	1 (11.1)
Age (Mean, SD)	31.67 (8.9)
Min-Max age (years)	19-42
Delay from beginning of symptoms	
Delay (Mean, SD)	24.56 (8.8)
Clinical symptoms	
Highest body Temperature (°C, mean, SD)	38.98 (0.4)
Constitutional symptoms	
Chills and/or sweats (n,%)	9 (100)
Aches (n,%)	9 (100)
Fatigue (n,%)	9 (100)
Headache (n,%)	8 (88.9)
Respiratory symptoms	
Cough (n,%)	7 (77.8)
Pharyngitis (n,%)	3 (33.3)
Sore throat or nasal congestion (n,%)	6 (66.7)
Other symptoms	
Expectoration (n,%)	1 (11.1)
Otitis (n,%)	0 (0.0)
Digestive disturbance (n,%)	0 (0.0)

Table S1. Demographic and clinical characteristics of patients included in the study.

Samples were obtained in the context of a previous clinical trial conducted in France during the A(H1N1)pdm09 pandemic, aimed at evaluating the antiviral efficacy and tolerability of classic antiviral monotherapy versus bitherapy (Escuret et al., 2012).

Molecules	Pharmalogical class
Monensin*	Antifungal Agents/Antiprotozoal Agents/Coccidiostats/Proton Ionophores/Sodium Ionophores
Isoxicam	Anti-Inflammatory Agents, Non-Steroidal
Iloprost*	Platelet Aggregation Inhibitors/Vasodilator Agents
Securinine	Alkaloids/GABAA Receptor Antagonists
Prestwick-692	Steroid Alkaloids
Biperiden*	Antiparkinson Agents/Muscarinic Antagonists/Parasympatholytics
Clorsulon	Anthelmintics/Antiplatyhelminic Agents
Felbinac	Anti-Inflammatory Agents, Non-Steroidal
Chenodeoxycholic acid*	Cathartics/Gastrointestinal Agents
Sulfamonomethoxine	Anti-Infective Agents
3-acetamidocoumarin	?
Meteneprost	Abortifacient Agents, Nonsteroidal
Adiphenine	Parasympatholytics/Anticholinergics/Antispasmodics
Benzathine benzylpenicillin	Anti-Bacterial Agents
Gentamicin	Anti-Bacterial Agents/Protein Synthesis Inhibitors
Timolol*	Adrenergic beta-Antagonists/Anti-Arrhythmia Agents/Antihypertensive Agents
Atractyloside*	Enzyme Inhibitors
Nadolol	Adrenergic beta-Antagonists/Anti-Arrhythmia Agents/Antihypertensive Agents/Sympatholytics
Lycorine*	Alkaloids/Protein Synthesis Inhibitors
Tranexamic acid*	Antifibrinolytic Agents
Lanatoside C	Anti-Arrhythmia Agents
Podophyllotoxin*	Antineoplastic Agents, Phytogenic/Keratolytic Agents/Tubulin Modulators
Alpha-estradiol*	5alpha-reductase inhibitors/Androgenic alopecia treatment
Alprostadi	Fibrinolytic Agents/Platelet Aggregation Inhibitors/Vasodilator Agents
Apigenin*	Anti-Inflammatory Agents, Non-Steroidal/?
Pipenzolate bromide	Muscarinic Receptor Antagonists
Amiloride*	Epithelial Sodium Channel Blockers/Diuretics/Acid Sensing Ion Channel Blockers
STOCK1N-35696	?
Carmustine	Antineoplastic Agents, Alkylating
PF-00539745-00	?
Clofilium tosylate	Anti-Arrhythmia Agents
Prestwick-983*	Antimetabolites/Antiviral Agents
Prestwick-675	Anthelmintics/Anticestodal Agents/Antiprotozoal Agents/Tubulin Modulators
Atracurium besilate	Neuromuscular Nondepolarizing Agents/Nicotinic Antagonists
Xamoterol	Adrenergic beta-1 Receptor Agonists
Demecarium bromide	Cholinesterase Inhibitors
Iopromide	Contrast Media
Etilefrine	Adrenergic alpha-Agonists/Adrenergic beta-1 Receptor Agonists/Cardiotonic Agents/Sympathomimetics/Vasoconstrictor Agents
Iproniazid	Antidepressive Agents/Monoamine Oxidase Inhibitors
Ketotifen*	Anti-Allergic Agents/Antipruritics/Histamine H1 Antagonists
Gly-His-Lys	Anti-Inflammatory Agents, Non-Steroidal?
Canadine*	Anti-Arrhythmia Agents/Calcium Channel Blockers/Platelet Aggregation Inhibitors
Viomycin	Anti-Bacterial Agents/Antibiotics, Antitubercular/Protein Synthesis Inhibitors

Disopyramide	Anti-Arrhythmia Agents/Voltage-Gated Sodium Channel Blockers
Fusidic acid	Anti-Bacterial Agents/Protein Synthesis Inhibitors
Amiprilose	Adjuvants, Immunologic/Anti-Inflammatory Agents, Non-Steroidal/Antiviral Agents
Anisomycin*	Anti-Bacterial Agents/Antiprotozoal Agents/Nucleic Acid Synthesis Inhibitors/Protein Synthesis Inhibitors
Ajmaline	Anti-Arrhythmia Agents
Arecoline	Cholinergic Agonists
Metampicillin	Anti-Bacterial Agents
Lasalocid	Anti-Bacterial Agents/Coccidiostats/Ionophores
Tolnaftate	Antifungal Agents
Metixene	Muscarinic Receptor Antagonists
PF-00539758-00	?
Streptomycin	Anti-Bacterial Agents/Protein Synthesis Inhibitors
Sulfapyridine	Anti-Infective Agents/Dermatologic Agents
Pivmecillinam	Anti-Bacterial Agents/Anti-Infective Agents, Urinary
Ribavirin*	Antimetabolites/Antiviral Agents
Prestwick-642*	Dermatologic Agents/Teratogens
Bumetanide	Diuretics/Sodium Potassium Chloride Symporter Inhibitors
Prednisone	Anti-Inflammatory Agents/Antineoplastic Agents, Hormonal/Glucocorticoids
Doxylamine	Antiemetics/Histamine H1 Antagonists
Diphenylpyraline	Histamine H1 Antagonists
Finasteride	5-alpha Reductase Inhibitors
Rosiglitazone*	Hypoglycemic Agents
15-delta prostaglandin J2	Anti-Inflammatory Agents, Non-Steroidal?/NFkB inhibitor?
5230742	?
Chloropyramine	Histamine H1 Antagonists
Prestwick-685	Anti-Inflammatory Agents, Non-Steroidal/Coloring Agents/Leprostatic Agents
Nimesulide*	Anti-Inflammatory Agents, Non-Steroidal/Cyclooxygenase Inhibitors
Morantel	Anthelmintics/Antinematodal Agents
Tropicamide	Muscarinic Receptor Antagonists/Mydriatics
Piperidolate	Muscarinic Receptor Antagonists
Riboflavin*	Photosensitizing Agents/Vitamin B Complex
Methoxamine	Adrenergic alpha-1 Receptor Agonists/Sympathomimetics/Vasoconstrictor Agents
Hydrocotarnine	Alkaloids/?
Propidium iodide	Coloring Agents/Indicators and Reagents/Intercalating Agents
Tolazoline	Adrenergic alpha-Antagonists/Antihypertensive Agents/Vasodilator Agents
5279552	?
Sulfadimethoxine	Anti-Infective Agents
N-acetyl-L-leucine	<i>Vertigo treatment/?</i>
Gibberellic acid	Plant Growth Regulators
Clorgiline	Antidepressive Agents/Monoamine Oxidase Inhibitors
Genistein	Anticarcinogenic Agents/Phytoestrogens/Protein Kinase Inhibitors
Pargyline	Antihypertensive Agents/Monoamine Oxidase Inhibitors
Cortisone	Anti-Inflammatory Agents
Medrysone	Anti-inflammatory Agents/Glucocorticoids
Isflupredone	Anti-inflammatory Agents/Mineralcorticoids

Prestwick-1082	?
Aciclovir*	Antiviral Agents
Sulconazole	Antifungal Agents
Cycloserine	Anti-Infective Agents, Urinary/Antibiotics, Antitubercular/Antimetabolites
Procainamide	Anti-Arrhythmia Agents/Voltage-Gated Sodium Channel Blockers
Chlortalidone	Antihypertensive Agents/Diuretics/Sodium Chloride Symporter Inhibitors
Chlorzoxazone	Muscle Relaxants, Central
Oxolamine	Antitussive Agents
Folic acid	Hematinics/Vitamin B Complex
Furazolidone	Anti-Infective Agents, Local/Anti-Infective Agents, Urinary/Antitrichomonal Agents/Monoamine Oxidase Inhibitors
Cotinine	Indicators and Reagents
Ikarugamycin*	Anti-Infective Agents
H-7	Enzyme Inhibitors
Natamycin	Anti-Bacterial Agents/Anti-Infective Agents, Local/Antifungal Agents
H-89*	Protein Kinase Inhibitors
Guanadrel	Antihypertensive Agents
Midodrine	Adrenergic alpha-1 Receptor Agonists/Sympathomimetics/Vasoconstrictor Agents
Etiocholanolone	Ketosteroids
Methyldopate	Antihypertensive Agents
Oxymetazoline*	Adrenergic alpha-Agonists/Nasal Decongestants/Sympathomimetics
Levomepromazine	Analgesics, Non-Narcotic/Antipsychotic Agents/Dopamine Antagonists
Thapsigargin	Enzyme Inhibitors
Pyrrithyldione	Psychoactive drugs
Nicergoline	Adrenergic alpha-Antagonists/Nootropic Agents/Vasodilator Agents
Apramycin	Anti-Bacterial Agents
Prestwick-1103	Anti-Inflammatory Agents, Non-Steroidal/Cyclooxygenase Inhibitors
Fenoprofen	Anti-Inflammatory Agents, Non-Steroidal/Cyclooxygenase Inhibitors
Fludrocortisone	Mineralocorticoids/Anti-Inflammatory Agents
Diphenhydramine	Anesthetics, Local/Anti-Allergic Agents/Antiemetics/Histamine H1 Antagonists/Hypnotics and Sedatives
Naloxone	Narcotic Antagonists
Benzonatate	Antitussive Agents
Thiocolchicoside	Muscle Relaxants
Eucatropine	Mydriatics
Dextromethorphan	Antitussive Agents/Excitatory Amino Acid Antagonists
Isometheptene	Adrenergic alpha-1 Receptor Agonists/Sympathomimetics/Vasoconstrictor Agents
Cinoxacin	Anti-Infective Agents
Levamisole*	Adjuvants, Immunologic/Antinematodal Agents/Antirheumatic Agents
Ursodeoxycholic acid	Cholagogues and Cholereitics
4,5-dianilinophthalimide	Protein Kinase Inhibitors
Ifenprodil	Adrenergic alpha-Antagonists/Excitatory Amino Acid Antagonists/Vasodilator Agents
CP-320650-01	?
Roxithromycin	Anti-Bacterial Agents
Lisuride	Antiparkinson Agents/Dopamine Agonists/Serotonin Receptor Agonists
lomefloxacin	Anti-Infective Agents
lorglumide	Hormone Antagonists

Piretanide	Diuretics/Sodium Potassium Chloride Symporter Inhibitors
L-methionine sulfoximine*	Enzyme Inhibitors
Diltiazem	Antihypertensive Agents/Calcium Channel Blockers/Cardiovascular Agents/Vasodilator Agents
Tyloxapol	Detergents/Surface-Active Agents
Flumequine	Anti-Infective Agents/Anti-Infective Agents, Urinary
Terazosin	Adrenergic alpha-1 Receptor Antagonists
Triflusal	Platelet Aggregation Inhibitors
Ranitidine	Anti-Ulcer Agents/Histamine H2 Antagonists
Flucytosine*	Antifungal Agents/Antimetabolites
Etomidate	Anesthetics, Intravenous/Hypnotics and Sedatives
Dioxybenzone	<i>UVB/UVA protection?</i>
Furaltadone	Anti-Infective Agents, Urinary
Ornidazole	Amebicides/Antitrichomonal Agents/Radiation-Sensitizing Agents
Dicloxacillin	Anti-Bacterial Agents
Pindolol	Adrenergic beta-Antagonists/Antihypertensive Agents/Serotonin Antagonists/Vasodilator Agents
Tretinoin*	Antineoplastic Agents/Keratolytic Agents
Proscillaridin	Cardiotonic Agents/Enzyme Inhibitors
Ouabain*	Cardiotonic Agents/Enzyme Inhibitors
Beclometasone	Anti-Asthmatic Agents/Anti-Inflammatory Agents/Glucocorticoids
Mexiletine	Anti-Arrhythmia Agents/Voltage-Gated Sodium Channel Blockers
Buflomedil	Vasodilator Agents
Levobunolol	Adrenergic beta-Antagonists/Sympatholytics
PHA-00851261E	?
Estropipate	Contraceptive Agents
Ioversol	Contrast Media
0175029-0000	?
Gelsemine	Alkaloids/?

Table S2. List of 160 selected molecules and their documented pharmacological classes. The 35 selected compounds for *in vitro* and *in vivo* evaluation are highlighted in grey. Asterisks (*) indicate molecules previously evaluated for their antiviral properties against influenza viruses or other viruses according to the literature, and question marks (?) indicate absence of assigned pharmacological class. Documented pharmacological classes were obtained from PubChem (<https://pubchem.ncbi.nlm.nih.gov>).

Molecule	CMAP (μM)	EC50 (nM)
Monensin	6	3.27
Biperiden	11	0.38
Felbinac	19	34.35
Sulfamonomethoxine	14	0.28
Adiphenine	11	6.29
Benzathin Benzylpenicilline	4	0.26
Gentamycin	3	0.039
Timolol	9	nd
Lanatoside C	4	nd
Alpha-estradiol	0.01	nd
Apigenin	15	0.21
Amiloride	13	0.41
Ribavirin	16	0.86
Methoxamine	16	nd
Tolazoline	20	0.93
Folic acid	9	0.22
Diphenhydramine	14	0.25
Roxythromycin	5	0.14
Pindolol	16	0.79
Prestwick-1103	20	626.63
Carmustine	100	0.07
Clofilium tosylate	8	0.16
Prednisone	11	nd
Choropyramine	12	0.07
Urseodeoxycholic acid	10	0.61
Ranitidine	11	0.68
Flucytosine	31	2.02
Diltiazem	9	0.84
Fusidic acid	7	0.038
Levamisole	17	nd
Sulfadimethoxine	13	0.69
Riboflavine	11	nd
Genistein	10	1.06
Nimesulide	13	nd
Etilefrine	18	0.34

Table S3. List of 35 selected molecules. CMAP concentration (μM) and calculated EC50 in the context of pre-treatment/treatment *in vitro*.

Influenza virus	Treatment	Dose	Viral titer (log TCID ₅₀ /ml)	Relative Viral production (% of mock-treated)
A/Lyon/969/2009 H275Y (H1N1) MOI 0.1	Diltiazem	0	4.8	100
		CMAP/10	3.97	14.7
		CMAP	2.8	1.0
	Etilefrine	0	4.63	100
		CMAP/10	3.97	22.0
		CMAP	2.8	1.5
A/Texas/126/2016 (H3N2) MOI 0.01	Diltiazem	0	6.02	100
		CMAP/10	5.13	12.75
		CMAP	4.92	7.9
	Etilefrine	0	5.63	100
		CMAP/10	4.8	14.7
		CMAP	3.63	1
B/Massachusetts/2/2106 MOI 0.1	Diltiazem	0	5.3	100
		CMAP/10	4.3	10.0
		CMAP	3.97	4.7
	Etilefrine	0	5.13	100
		CMAP/10	4.3	15.0
		CMAP	3.97	7.3

Table S4. Evaluation of antiviral efficacy of diltiazem or etilefrine in the context of infection by different influenza strains. Human lung epithelial cells (A549) were incubated with supplemented medium (mock), or different concentrations of diltiazem (CMAP, 9 μ M) or etilefrine (CMAP, 18 μ M). Six hours after treatment, cells were washed and then infected with different prototype human influenza strains (as indicated). One hour after viral infection, a second identical treatment dose in supplemented medium was added. Relative viral titers compared to the mock-treated control are shown. Results are representative of two independent experiments, and confirm the antiviral activity of diltiazem and etilefrine on oseltamivir-resistant A(H1N1)pdm09, as well as wild-type H3N2 and B influenza strains.

Pre-incubation treatment	Viral titer (log TCID50/ml)		Mean relative Viral production (% of mock-treated)
	Dilution #1	Dilution #2	
Control PBS	5.3	4.63	-
Diltiazem (9 μ M)	5.63	4.63	156.9
Etilefrine (18 μ M)	5.30	4.63	100.0
Oseltamivir (1 μ M)	5.63	4.30	130.3
Negative serum	4.97	4.30	47.7
Positive serum	3.30	2.53	0.9

Table S5. Virus pre-incubation with diltiazem or etilefrine does not interfere with early viral entry steps. Two viral dilutions (#1 and #2, respectively 10^6 and 10^5 TCID50/mL) were pre-incubated for 1 h with PBS, diltiazem (CMAP, 9 μ M), etilefrine (CMAP, 18 μ M), or oseltamivir (1 μ M). A(H1N1)pdm09 positive and a negative sera were used as controls. After incubation, viral titers (log₁₀ TCID50/mL) were determined in MDCK cells. Results are representative of two independent experiments and indicate that pre-incubation with either diltiazem or etilefrine does not affect viral titers compared to PBS-incubated control, suggesting that the antiviral effect of these molecules is not mediated by direct drug-virus interactions at early stages of viral entry.

Hours P.I.	Treatment	Apical viral titer		Δ TEER
		PFU/ml	log TCID50/ml	Ohm/cm ²
		(CI95)	(CI95)	(CI95)
24	Mock	7.2 [^] 5 (2.3 [^] 5 – 1.2 [^] 6)	6.74 (6.53 – 6.95)	59.84 (-35.75 – 155.4)
	Oseltamivir 0.1 μ M	2.1 [^] 5 (1.6 [^] 4 – 4.1 [^] 5)	6.02 (4.69 – 7.35)	8.98 (-81.72 – 99.68)
	Oseltamivir 1 μ M	2.1 [^] 4*** (2.3 [^] 3 – 3.9 [^] 4)	5.13*** (4.61 – 5.66)	-24.32 (-58.00 – 9.36)
	Diltiazem 9 μ M	3.8 [^] 6 (1.6 [^] 5 – 6.0 [^] 5)	6.47 (5.03 – 7.90)	35.10 (10.96 – 59.23)
	Diltiazem 90 μ M	3.1 [^] 4*** (1.8 [^] 5 – 4.3 [^] 5)	5.57** (4.95 – 6.18)	86.13 (3.72 – 168.5)
	Ose 0.1 μ M / Dil 9 μ M	5.3 [^] 4*** (1.7 [^] 3 – 1.0 [^] 5)	6.25 (5.62 – 6.89)	34.50 (-33.15 – 102.2)
	Ose 1 μ M / Dil 90 μ M	2.3 [^] 4*** (1.9 [^] 4 – 2.7 [^] 4)	5.19*** (4.15 – 6.23)	32.96 (-77.24 – 143.2)
48	Mock	2.1 [^] 8 (1.3 [^] 8 – 3.0 [^] 8)	9.12 (8.91 – 9.33)	-2.64 (-233.3 – 228.0)
	Oseltamivir 0.1 μ M	5.9 [^] 7** (4.9 [^] 7 – 6.8 [^] 7)	8.61 (7.43 – 9.80)	20.09 (-39.75 – 79.94)
	Oseltamivir 1 μ M	8.8 [^] 4*** (3.2 [^] 3 – 1.7 [^] 5)	6.20*** (5.39 – 7.01)	7.26 (-85.73 – 100.3)
	Diltiazem 9 μ M	5.8 [^] 7** (3.0 [^] 7 – 8.5 [^] 7)	8.91 (8.67 – 9.16)	-48.31 (-180.1 – 83.47)
	Diltiazem 90 μ M	1.0 [^] 5*** (4.4 [^] 4 – 1.5 [^] 5)	6.56*** (5.23 – 7.88)	120.1 (-85.77 – 326.00)
	Ose 0.1 μ M / Dil 9 μ M	2.3 [^] 6*** (9.7 [^] 5 – 3.6 [^] 6)	7.54* (6.92 – 8.17)	78.28 (33.37 – 123.2)
	Ose 1 μ M / Dil 90 μ M	2.6 [^] 4*** (1.4 [^] 4 – 3.8 [^] 4)	5.38*** (5.05 – 5.71)	-8.84 (-58.73 – 41.05)
72	Mock	1.2 [^] 8 (3.3 [^] 7 – 2.1 [^] 8)	8.48 (8.02 – 8.94)	-244.1 (-275.2 – -213.0)
	Oseltamivir 0.1 μ M	4.6 [^] 7* (7.6 [^] 6 – 8.4 [^] 7)	8.30 (7.73 – 8.87)	-110.9* (-256.0 – 34.2)
	Oseltamivir 1 μ M	1.7 [^] 5*** (7.1 [^] 4 – 2.7 [^] 5)	6.85*** (6.14 – 7.56)	22.55*** (-20.25 – 65.35)
	Diltiazem 9 μ M	1.9 [^] 7** (-4.7 [^] 5 – 3.9 [^] 7)	8.21 (7.28 – 9.14)	-218.0 (255.6 – -180.4)
	Diltiazem 90 μ M	2.1 [^] 5*** (1.3 [^] 5 – 3.0 [^] 5)	7.38* (6.53 – 8.22)	-115.5 (-308.5 – 77.52)
	Ose 0.1 μ M / Dil 9 μ M	1.8 [^] 7** (6.9 [^] 6 – 2.8 [^] 7)	8.41 (7.38 – 9.45)	-37.88** (-215.3 – 139.6)
	Ose 1 μ M / Dil 90 μ M	4.7 [^] 4*** (3.8 [^] 4 – 5.7 [^] 4)	5.62*** (5.23 – 6.01)	-43.16** (-77.17 – -9.15)
96	Mock	2.8 [^] 7 (1.3 [^] 7 – 4.2 [^] 7)	7.86 (7.74 – 7.99)	-267.3 (-288.7 – -246.0)
	Oseltamivir 0.1 μ M	4.1 [^] 6*** (-2.3 [^] 6 – 1.0 [^] 7)	7.80 (6.56 – 9.04)	-209.2 (-271.5 – -146.8)
	Oseltamivir 1 μ M	1.8 [^] 5*** (6.3 [^] 3 – 3.4 [^] 5)	7.09 (5.79 – 8.40)	10.67*** (-27.47 – 48.81)
	Diltiazem 9 μ M	2.3 [^] 6*** (1.9 [^] 6 – 2.7 [^] 6)	7.32 (6.43 – 8.22)	-220.5 (-267.4 – -173.5)
	Diltiazem 90 μ M	1.6 [^] 5*** (-5.6 [^] 4 – 3.7 [^] 5)	7.37 (5.97 – 8.76)	24.59*** (-10.79 – 59.97)
	Ose 0.1 μ M / Dil 9 μ M	4.0 [^] 6*** (1.2 [^] 6 – 6.8 [^] 6)	7.84 (7.38 – 8.31)	-149.9* (-379.8 – 80.1)
	Ose 1 μ M / Dil 90 μ M	2.9 [^] 4*** (2.1 [^] 4 – 3.7 [^] 4)	5.47** (4.38 – 6.56)	-59.79*** (-97.62 – -21.96)

Table S6. Apical viral production and transepithelial electrical resistance (TEER) in infected MucilAir® human airway epithelium (HAE). MucilAir® HAE were infected on the apical pole with influenza A/Lyon/969/09 (H1N1)pdm09 virus at a MOI of 0.1 and treated on the basolateral pole. Treatments were initiated 5 h after infection and were continued once daily for 4 additional days. * $p < 0.05$, ** $p < 0.01$ and *** $p < 0.001$ compared to the infected mock-treated group by one-way ANOVA with Tukey's post-test. Data are representative of at least three independent experiments.